https://doi.org/10.5194/nhess-2022-183
Preprint. Discussion started: 6 July 2022

Natural Hazards and Earth System Sciences
Discussions

Scenario-based multi-risk assessment from existing single-hazard vulnerability models. An application to consecutive earthquakes and tsunamis in Lima, Peru

Juan Camilo Gómez Zapata[1, 2], Massimiliano Pittore[1, 3], Nils Brinckmann[4], Juan Lizarazo-Marriaga[5], Sergio Medina[5], Nicola Tarque[6, 7], and Fabrice Cotton[1, 2],

[1]Seismic Hazard and Risk Dynamics, GFZ German Research Centre for Geosciences, Potsdam, 14473, Germany
[2] Institute for Geosciences, University of Potsdam, Karl-Liebknecht-Str. 24-25, Potsdam, 14476, Germany
[3] Institute for Earth Observation, EURAC Research, Viale Druso 1, Bolzano, 39100, Italy
[4] eScience Centre, GFZ German Research Centre for Geosciences, Telegrafenberg, Potsdam, 14473, Germany
[5] Departamento de Ingeniería Civil y Agrícola, Universidad Nacional de Colombia, sede Bogotá, 11001, Colombia
[6] Gerdis Research Group, Civil Eng. Division, Pontificia Universidad Católica del Perú, Av. Universitaria 1801, Lima, Peru
[7] Department of Continues Mechanics and Structures, Universidad Politécnica de Madrid, Calle Aranguren 3, Madrid, Spain

Correspondence to: jcgomez@gfz-potsdam.de

Abstract. Multi-hazard risk assessments for building portfolios exposed to earthquake shaking followed by a tsunami are usually based on empirical vulnerability models calibrated on post-event surveys of damaged buildings. The applicability of these models cannot easily be extrapolated to other regions of larger/smaller events. Moreover, the quantitative evaluation of the damages related to each of the hazards type (disaggregation) is impossible. To investigate cumulative damage on extended building portfolios, this study proposes an alternative and modular method to probabilistically integrate sets of single-hazard vulnerability models that are being constantly developed and calibrated by experts from various research fields to be used within a multi-risk context. This method is based on the proposal of state-dependent fragility functions for the triggered hazard to account for the pre-existing damage, and the harmonisation of building classes and damage states through their taxonomic characterization, which is transversal to any hazard-dependent vulnerability. This modular assemblage also allows us to separate the economic losses expected for each scenario on building portfolios subjected to cascading hazards. We demonstrate its application by assessing the economic losses expected for the residential building stock of Lima, Peru, a megacity commonly exposed to consecutive earthquake and tsunami scenarios. We show the importance of accounting for damage accumulation on extended building portfolios while observing a dependency between the earthquake magnitude and the losses derived for each hazard scenario. For the commonly exposed residential building stock of Lima exposed to both perils, we find that classical tsunami empirical fragility functions lead to an underestimation of predicted losses for lower magnitudes (M_w) and large overestimations for larger Mw events in comparison to our state-dependent models and cumulative damage method.

https://doi.org/10.5194/nhess-2022-183
Preprint. Discussion started: 6 July 2022


Natural Hazards and Earth System Sciences Discussions

1. Introduction

Cascading natural events, commonly defined as a primary hazard triggering a secondary one, have jointly induced large disasters (Gill and Malamud, 2016). In the case of earthquakes, between 25 and 40% of economic losses and deaths have been reported to result as a consequence of secondary effects, i.e., tsunamis, landslides, liquefaction, fire, and others (Daniell et al., 2017). Well-known examples are the submarine earthquakes and the subsequent tsunamis occurred in 2004 in the India Ocean, in 2011 in Japan, and in 2018 in Palu Bay in Indonesia (Goda et al., 2019). These events not only induced cumulative physical damage on the exposed infrastructure, but also brought drastic socioeconomic cascading effects that are still perceptible today (de Ruiter et al., 2020; Suppasri et al., 2021). Despite the magnitude of such events, multi-hazard risk assessment remains a relatively new research field with still not unified terminologies and approaches (Pescaroli and Alexander, 2018; Tilloy et al., 2019). Nonetheless, a number of studies (e.g., Kappes et al., 2012; Komendantova et al., 2014; Gallina et al., 2016; Julià and Ferreira, 2021; De Angeli et al., 2022; Cremen et al., 2022) have unanimously agreed that more realistic multi-risk evaluations can only be conducted if both (1) multi-hazard (e.g., Marzocchi et al., 2012; Liu et al., 2016) and (2) multi-vulnerability interactions (e.g., Zuccaro et al., 2008; Gehl et al., 2013) are considered altogether. While the former comprises the study of the conditional probabilities of the occurrences of these hazards and their combination, the study of the latter involves reviewing the many classes of vulnerabilities that are associated with an exposed territory.

Therefore, in this study, we narrow down the scope by assuming that a second hazardous event is always triggered after the occurrence of the first one, thus eliminating the need to quantify the probability of this occurring. Thus, we will only focus on the dynamic physical vulnerability and related cumulative damage that a building stock exposed to a close succession of hazardous events might suffer.

In exposure modelling for multi-hazard risk purposes, we can distinguish between two main approaches:

1. Using a single set of building classes, each employing as many fragility/vulnerability models as the natural hazards considered, for example, the HAZUS-MH (FEMA, 2003, 2017); Dabbeek and Silva, (2020); and Dabbeek et al., (2020). They have typically associated sets of fragility functions with equivalent damage states regardless of the hazard. Aligned with this philosophy, the EMS-98 vulnerability classes (Grünthal, 1998) were used by some authors to not only describe the likely damage due to seismic action, but also to classify likely ranges of vulnerabilities to other hazards based on the building's material types (Schwarz et al., 2019; Maiwald and Schwarz, 2019).
2. Jointly applying a number of different building classifications per individual hazard to the same exposed buildings (e.g., Gómez Zapata et al., 2021e; Arrighi et al., 2022). Their associated fragility functions may have different sets of damage states (differing in number and description). Notably, these models are constantly developed and individually validated by experts of each research field.

Although the first type might be useful in the assessment of risk arising from independent hazards, their related sets of fragility models lack multi-hazard calibration and validation and, therefore, do not offer sufficient inputs for assessing the increasing damage from cascading events (Ward et al., 2020).

https://doi.org/10.5194/nhess-2022-183
Preprint. Discussion started: 6 July 2022


Natural Hazards and Earth System Sciences Discussions

Moreover, the definition of the damage scale depends on the building type (Hill and Rossetto, 2008) and the likely failure mechanisms that it can experience under the action of specific hazard intensity measures (IM) (Vamvatsikos et al., 2010; Selva, 2013). Therefore, the observable damage features on individual structural or non-structural components that jointly describe a certain damage state can have contrasting descriptions across various hazard-dependent vulnerability types (Gehl and D'Ayala, 2018; Figueiredo et al., 2021) and there is often not a 1:1 relation between them for the case of earthquakes and tsunamis (Bonacho and Oliveira, 2018; Lahcene et al., 2021). The reasons behind such a mismatching between the definitions of damage states may arise from the absence of standard formats for damage data collection across regions and across the several vulnerability types of interest (Mas et al., 2020; Frucht et al., 2021). Notably, the study of Negulescu et al., (2020) found this to be particularly significant for the multi-hazard risk context, stating that the damage states of earthquake and tsunami fragility models can have variable levels of compatibility. This assumption led to contrasting loss estimates with respect the U.S HAZUS approach, which is based on the complete equivalence between damage grades. This background portrays the need to standardise the description of the physical damage through harmonizing scales across several hazard-dependent vulnerabilities, which are inputs for unified methods in multi-hazard risk (Ward et al., 2022).

The earthquake engineering has investigated the cumulative damage expected during seismic sequences (e.g. Papadopoulos and Bazzurro, 2021; Karapetrou et al., 2016; Trevlopoulos et al., 2020), but this concept is rarely considered in other research disciplines. For instance, the physical vulnerability of building portfolios to tsunamis has been typically evaluated through empirical fragility functions derived from post-near-field tsunami surveys. A drawback of these functions is that they have been presented solely as tsunami fragility functions in terms of the inundation depth when in reality these surveys encompassed assets that experienced cumulative damage due to the joint effect of the tsunami-generating earthquake and the tsunami itself (Charvet et al., 2017). Due to this limitation, analytical fragility functions were recently proposed for individual structures (e.g., Attary et al., 2017) and for large-scale building stocks with generalised typologies (Belliazzi et al., 2021). However, as remarked by Attary et al., (2019), using these functions for loss estimation should only be valid for far-field tsunamis, and for near-field events the damage induced by shaking before the tsunami strikes must still be addressed.

To the best of the authors' knowledge, only a few studies have investigated the performance of heterogeneous and large-scale building portfolios for risk estimates subjected to consecutive ground shaking and tsunamis. Hereby, we summarize some of them. In Goda and De Risi, (2018) a rationale was proposed for adopting the larger value of the damage ratios from independent earthquake and tsunami risk computations. In Park et al., (2019) a probabilistic multi-risk approach was presented for a building stock in the USA subjected to spatially uncorrelated seismic ground motions and subsequent tsunamis. This study showed the disaggregation of losses per hazard and per material-based building type across several return periods while assuming statistical independence between their respective damage states. As a common denominator of the aforementioned studies, the cumulative damage and losses from a building portfolio were not assessed. Since these metrics cannot be obtained as the sum of the effects from each individual hazardous event (Bernal et al., 2017; Terzi et al., 2019), it is rather necessary to address the nonlinear damage accumulation on the same exposed assets during the multi-hazard sequences (Merz et al., 2020).

https://doi.org/10.5194/nhess-2022-183
Preprint. Discussion started: 6 July 2022


Natural Hazards and Earth System Sciences Discussions

This study contributes to the field by proposing a modular method to to probabilistically integrate sets of single-hazard vulnerability models that are being constantly developed and calibrated by experts from various research fields to be used within a multi-risk context, solve the harmonization problem between existing seismic and tsunami building classification schemes and harmonize the damage state definitions within the two single-hazard vulnerability models. This is done with the purpose of representing the damage distribution resulting after the earthquake (shaking) phase through a damage-updated exposure model whose damage scale is dependent on the classification scheme required for assessing the vulnerability to a triggered (tsunami) event. Complementary, we propose to use state-dependent fragility models that account for the pre-existing damage caused by the first event (shaking). These modules are valuable inputs for ultimately assessing the expected cumulative damage that is expected in consecutive hazard scenarios. We demonstrate the application of this method by investigating the likely cumulative damage on the residential buildings of Lima (Peru) by considering this city's exposure to six mega-thrust earthquake scenarios (main shock) and subsequent tsunamis. Every damage distribution is translated into direct economic losses to gain a comparative risk metric and disaggregate the contribution of each hazard scenario.

2. Proposed method

To assess the cumulative damage that is expected to be experienced by a building portfolio during hazardous event sequences, we rely on the principle that its related exposure model is represented by jointly applying existing building classification schemes, one per each individual hazardous scenarios of the cascading sequence. For example, one building that is expected to be affected by a first intensity IM^A (e.g., ground-shaking) and a second one IM^B (e.g., tsunami inundation) is actually classified under two exposure classification schemes (T_k^A and T_j^B), respectively, which have attached their related vulnerability modes (Figure 1a). Each scheme contains a set of mutually exclusive, collectively exhaustive building classes $k = \{k_1, \dots, k_n\}$ and $j = \{j_1, \dots, j_n\}$ correspondingly.

To assess the expected damage state after the first hazardous event (e.g., ground-shaking), we apply their fragility function $\sum_z p(D_{kz}^A|IM^A)$ which give us the probability that a building k, typically assumed to be in an undamaged state 0, (D_{k0}^A), changes to a progressive state z due to a hazard intensity IM^A (green part in Figure 1b). For risk assessment, this is completed by the consequence model ($L|D_{kz}^A$), which assigns a loss ratio L of the total replacement cost of class k given the occurrence of a damage state. Thus, the expected loss given a hazard intensity IM^A is calculated considering the contributions from all possible damage states and their probabilities, as per Eq. 1.

$$p(L|IM^A) = \sum_z p(D_{kz}^A|IM^A)p(L|D_{kz}^A) \quad \text{Eq. 1}$$

If this damaged building portfolio is subjected to the action of a second scenario with a hazard intensity IM^B, it would experience cumulative damage moving from a damage state z, (D_{kz}^A) to a damage state w (but in the domain of the second vulnerability scheme: D_{jw}^B). Due to this differential scheme classification, their respective set of damage states may not have

https://doi.org/10.5194/nhess-2022-183
Preprint. Discussion started: 6 July 2022

Natural Hazards and Earth System Sciences
Discussions

trivial equivalences because they can also have different observable damage features. Therefore, we propose integrating a set of modular components, namely: **(1)** inter-scheme compatibilities between each hazard-dependent exposure classification scheme $p\left(T_k^A|T_j^B\right)$ (i.e., purple part in Figure 1b, method originally proposed in Gómez Zapata et al., (2022b), and summarised in Sect. 2.1). Moreover, since the fragility models attached to such schemes may have different numbers of damage states and descriptions, we also propose to obtain **(2)** their related compatibility levels between inter-scheme damage states $p\left(D_{kz}^A|D_{jy}^B\right)$ (i.e., red part in Figure 1b, explained in Sect. 2.2). Through these conversions, the damaged updated exposure model resulting from the action of IM^A can be represented in the domain of the reference scheme attached to the second vulnerability to be analysed. Complementary, **(3)** single-hazard state-dependent fragility functions (with non-zero initial damage states) are incorporated to calculate the cumulative damages expected after the triggered event with IM^B, while accounting for the preceding induced by IM^A (i.e., blue part in Figure 1b, developed in Sect. 2.3). For risk assessment, (4) the incremental loss obtained from the economic consequence model attached to the classification scheme T_j^B (i.e., replacement costs and related loss ratios per D_{jy}^B) is integrated (i.e., yellow part in Figure 1b, explained in Sect. 2.4). These modules are described hereafter.

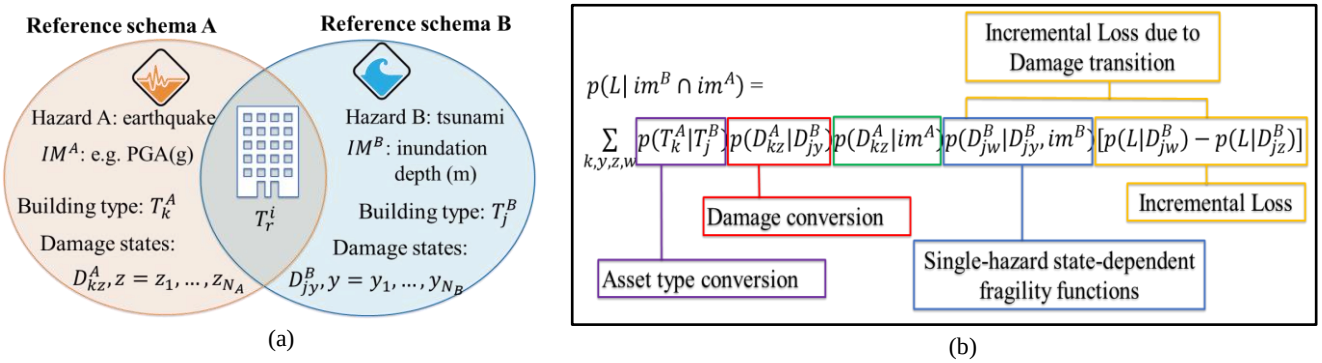

Figure 1. (a) Example of the principle proposed for classifying the same building class into two hazard-dependent reference schemes with associated fragility models. (b) Schematic representation of the proposed method that is developed afterward.

2.1 Exposure modelling: taxonomic description, inter-scheme conversion and spatial aggregation of building classes

The classified building stock under the first hazard-dependent classification scheme T_k^A is spatially aggregated into a set of geocells that capture the local spatial variations of the hazards' IM of interest across the study area. For such a purpose, we recommend using variable resolution exposure models in the form of Central Voronoi Tessellations (CVT). Besides spatially representing the building portfolio, they also provide a representative IM per geocell for reliable and computationally efficient vulnerability estimations (Pittore et al., 2020; Gómez Zapata et al., 2021e). They also implicitly serve as common minimum reference units (MRU) aggregation entities between exposure and hazard (Zuccaro et al., 2018). This is because for their derivation, one can consider the combination of local variations of the hazard intensity measures (IM) and certain

https://doi.org/10.5194/nhess-2022-183
Preprint. Discussion started: 6 July 2022


Natural Hazards and Earth System Sciences Discussions

exposure proxies (e.g., population density) across the same area. CVT-based models may be useful in a multi-hazard risk context where the spatial correlation of various IM can differ (e.g., ground-shaking and tsunami inundation) (Gill and Malamud, 2014).

As shown in Pittore et al., (2018), every building class *k* that belongs to one scheme *A* can be described in terms of basic observable features $\{F\}_m$ within a faceted taxonomy, that is, a building classification schema in which building classes result from the characterisation of individual attributes, or facets (Brzev et al., 2013; Silva et al., 2018, 2022). This disaggregation is the common underlying vocabulary to obtain the probability that a building class within the source scheme (T_k^A) corresponds to another class within the target scheme $\left(T_j^B\right)$. As proposed in Gómez Zapata et al., (2022b), the degree of compatibility between the buildings classes belonging to both schemes can represented by a compatibility matrix $p\left(T_k^A|T_j^B\right)$ to account for the uncertainties when there is not a trivial (one-to-one) mapping. Knowing in advance certain exposure metrics of the source scheme $\{R\}_{T_k^A}$ (i.e., building counts), the respective values of the target scheme $\{R\}_{T_j^B}$ are obtained by applying the dot product (Eq. 2).

$$\{R\}_{T_j^B} = p\left(T_k^A|T_j^B\right).\{R\}_{T_k^A} \quad \text{Eq. 2}$$

2.2 *The probabilistic description and compatibility of inter-scheme damage states*

We consider how the fragility functions associated with T_k^A and T_j^B may have diverse numbers and descriptions of damage states per considered hazard-dependent vulnerability scheme ($D_{kz}^A, z = z_1, \dots, z_{N_A}$ and $D_{jy}^B, y = y_1, \dots, y_{N_B}$). To harmonise their equivalence, we propose obtaining their probabilistic inter-scheme compatibility as a set of matrices $p\left(D_{kz}^A|D_{jy}^B\right)$. This is achieved after having evaluated how the likely observable characteristics linked to each damage state within D_{kz}^A and D_{jy}^B can be expressed in terms of another one. For this aim, we first propose the use of the AeDES form (Agibilità E Danno in Emergenza Sismica (usability and damage in seismic emergency)) of the Italian Civil Protection (Baggio et al., 2007) as a standard scoring system to create a synthetic dataset based on the likely observable damage on individual building components. Although it was originally proposed for post-earthquake damage data collection, we propose to transversally use it to describe every damage state z and y of D_{kz}^A and D_{jy}^B, respectively. Expert elicitation is used on the AeDES form to create heuristics evaluating the expected damage extension per building type and damage-limit-states. For this aim, we make use of its implicit scale within a range of 0=L to 9=A over the building components n, (low-level taxonomic attributes) as shown in Figure 2. We decided to only include four out of these six components that can be found in any building type as listed in Eq. 3 as stairs and pre-existing damage are not always present in all buildings. The importance of such building components for assessing their physical vulnerability has been documented in previous studies to ground-shaking (e.g. Lagomarsino et al., 2021) and tsunamis (e.g. Del Zoppo et al., (2021)).

$$n = \{vertical\ structure\ (VS); floor\ (FL); roof\ (RF); infills\ and\ partitions\ (IP)\} \quad \text{Eq. 3}$$

https://doi.org/10.5194/nhess-2022-183
Preprint. Discussion started: 6 July 2022

Natural Hazards and Earth System Sciences
Discussions

Damage level - extension / Structural component Pre-existing damage		DAMAGE (1)									
		D4-D5 Very Heavy			D2-D3 Medium-Severe			D1 Light			Null
		> 2/3	1/3 - 2/3	< 1/3	> 2/3	1/3 - 2/3	< 1/3	> 2/3	1/3 - 2/3	< 1/3	
		A	B	C	D	E	F	G	H	I	L
1	Vertical structures	☐	☐	☐	☐	☐	☐	☐	☐	☐	○
2	Floors	☐	☐	☐	☐	☐	☐	☐	☐	☐	○
3	Stairs	☐	☐	☐	☐	☐	☐	☐	☐	☐	○
4	Roof	☐	☐	☐	☐	☐	☐	☐	☐	☐	○
5	Infills and partitions	☐	☐	☐	☐	☐	☐	☐	☐	☐	○
6	Pre-existing damage	☐	☐	☐	☐	☐	☐	☐	☐	☐	○

Figure 2. Scale to assess the damage level on buildings as proposed by the AeDES form. Reprinted from Baggio et al, 2007.

A heuristic is generated by scoring the four components in Eq. 3 per damage state, per fragility function, per building class of both exposure classification schemes. This is done through expert elicitation and establishes a training dataset of the possible observable damage extent $\{OD\}_n$ in a harmonized manner. For instance, one set of $\{OD\}_n$ (for a given damage state and building type) is made up by a set of four numbers from 0 to 9, e.g., n = {1, 2, 1, 3}, meaning level I for VS and RF, level H for FL and level G for IP (Eq. 3). Thereafter, using the total probability theorem, the probability that the damage state z of a building class j in a scheme A corresponds to damage state y of building class j in scheme B can be calculated by Eq. 4.

$$p\left(D_{kz}^{A}|D_{jy}^{B}\right) = \sum_{n} p\left(D_{kz}^{A}|\{OD\}_n \cap D_{jy}^{B}\right) p\left(\{OD\}_n|D_{jy}^{B}\right) \quad \text{Eq. 4}$$

We assume that the representations of damage states within the two considered schemes are conditionally independent (⫫). Thereby, given the information of the scored observable damage on the individual components $\{OD\}_n$, we can describe the source damage scheme D_{kz}^{A} to be modelled in terms of $\{OD\}_n$ that jointly compose the target scheme D_{jy}^{B}: $D_{jz}^{A} \perp\!\!\!\perp D_{jy}^{B}|\{OD\}_n$.Thus, Eq. 4 can be expressed as a product, given by Eq. 5.

$$p\left(D_{kz}^{A}|D_{jy}^{B}\right) = \sum_{n} p\left(D_{kz}^{A}|\{OD\}_n\right) p\left(\{OD\}_n|D_{jy}^{B}\right) \quad since\ D_{kz}^{A} \perp\!\!\!\perp D_{jy}^{B}|\{OD\}_n \quad \text{Eq. 5}$$

We obtain a probabilistic compatibility degree between damage states ($D_{kz}^{A}, z = z_1, \dots, z_{N_A}$ and $D_{jy}^{B}, y = y_1, \dots, y_{N_B}$) for every pair of combination of building classes T_k^A, and T_j^B through a Bayesian formulation as presented in Eq. 6.

$$p\left(D_{kz}^{A}|D_{jy}^{B}\right) = \sum_{n} p\left(D_{kz}^{A}|\{OD\}_n\right) p\left(D_{jy}^{B}|\{OD\}_n\right) \frac{p(\{OD\}_n)}{p\left(D_{jy}^{B}\right)} \quad \text{Eq. 6}$$

The terms $p(D_{kz}^{A}|\{OD\}_n)$ and $p\left(D_{jy}^{B}|\{OD\}_n\right)$ in Eq. 6 can be solved through supervised machine learning techniques for classification (e.g., logistic regression, naive Bayes, decision trees) to predict the probabilities between the training sets

https://doi.org/10.5194/nhess-2022-183
Preprint. Discussion started: 6 July 2022


Natural Hazards and Earth System Sciences Discussions

and a synthetic testing dataset. The selection of the machine learning technique, naturally, carries epistemic uncertainties (Mangalathu et al., 2020) whose investigation is beyond the scope of this study. The testing dataset is obtained after generating random numbers of all the possible combinations of the AeDES-based scores. With this dataset we express the conditional probabilities of having damage states D_{kz}^{A}, z and D_{jy}^{B}, y (for each building class within schemes A and B given $\{OD\}_n$. The term $p(\{OD\}_n)$ is a marginal probability that can be assumed to represent the proportion of one observation out of exhaustive combinations of $\{OD\}_n$. Lastly, $p\left(D_{jy}^{B}\right)$ describes the proportion of each damage state y within each building class k in the training dataset for scheme B. Once Eq. 6 is solved, the expression $p\left(D_{kz}^{A}|D_{jy}^{B}\right)$ is obtained, which stems from the probabilistic inter-scheme damage compatibility matrix for each possible pair of buildings within schemes A and B. After having established the compatibility between building classes and damage states, a special set of fragility functions is needed to follow the damage progression inflicted by the second hazard. They are explained hereafter.

2.3 State-dependent fragility functions

The next steps of the method are carried out within the reference vulnerability scheme of the second hazard. Let us suppose that the damage state w belongs to $D_{jy}^{B}, y = y_1, \dots w \dots, y_{N_B}$. Eq. 7 represents the conditional probability that the building j (of the scheme B) can move to a progressive state w given the action of IM^B when it already presented a damage state y due to the action of IM^A. For such a process, it was already classified in terms of scheme B, thanks to the compatibilities between damage states from different scales described above.

$$p\left(D_{jw}^{B}|D_{jy}^{B}, IM^{B}\right) \quad \text{Eq. 7}$$

The former expression defines a probabilistic state-dependent fragility function composed of transition probabilities between increasing damage states. For instance, for the scheme B, this description follows: $y_{N_B} - y_{N_B-(N_B-1)}; y_{N_B} - y_{N_B-(N_B-2)}$ ... For a fragility model $D_{T_r^i}$ designed for a set of building types T_r, and composed of q_{N_i} damage states (for any hazard of interest i), the required set of transition probabilities for a given range of hazard intensities are completely defined by a triangular number G_f as expressed in Eq. 8.

$$G_f = \sum_{D_{T_r^i}=1}^{q_{N_i}} D_{T_r^i} = \frac{\left(1 + q_{N_i}\right) q_{N_i}}{2} \quad \text{Eq. 8}$$

If a fragility function is composed of $q_{N_i} = 3$ damage states (excluding damage state 0, equivalent to no damage), the required triangular number to express the damage state transitions is $G_f = 6$ (3 from 0; 2 from 1: 1 from 2). A visual example of such transition probabilities within fragility functions for several hazard-dependent models (also including T_k^A; T_j^B and their respective sets of damage states z_{N_A}; y_{N_B} is presented in Figure 3. For each T_r^i, it is then necessary to determine the

https://doi.org/10.5194/nhess-2022-183
Preprint. Discussion started: 6 July 2022

Natural Hazards and Earth System Sciences
Discussions

probabilistic representation of the damage state transitions in every G_f that forms the damage-state fragility functions. For that aim, the relation proposed in Mignan et al., (2014) expressed in Eq. 9 is adopted.

$$\delta_{w|y} = \frac{1}{2} erfc\left(\frac{-ln(d_w) - \mu_{w|y}}{\sigma_w\sqrt{2}}\right) \quad \text{Eq. 9}$$

This relation proposes that the lognormal cumulative distribution $\delta_{w|y}$ be used to find a damage state w conditional on the previous occurrence of damage state y. It describes the conditional transition probabilities of exceedance between damage states. Every mean value of the damage transitions $\mu_{w|y}$ of D_{jy}^B can be expressed as $\mu_{w|y} = \mu_w - \varphi ln(d_y)$, where d_w and d_y are the corresponding IM to the damage states w and y, and φ represents the scaling factors that modify the fragility function and shifts to higher probabilities of exceeding a given damage state for the same hazard intensity IM^B. The scaling factors φ are obtained as ad-hoc calibration parameters, similarly as proposed in Mignan et al., (2014). The fragility functions used to constrain the state-dependent fragility functions should have been derived only for the actual second acting hazard (i.e., far-field tsunamis). Thus, the use of those derived analytically is advised over empirical ones (which had implicit the damaged induced by ground-shaking in their derivation).

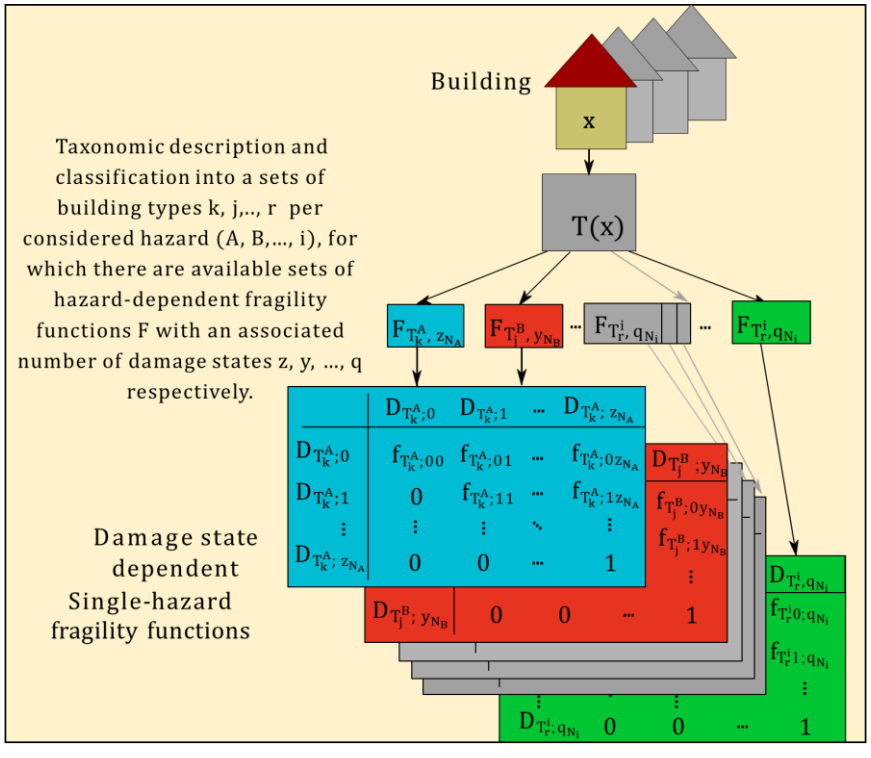

Figure 3. Example of a set of damage state-dependent fragility functions for several single hazard fragility functions comprising progressive transition probabilities. Figure modified from Gómez Zapata et al., (2020).

https://doi.org/10.5194/nhess-2022-183
Preprint. Discussion started: 6 July 2022


Natural Hazards and Earth System Sciences Discussions

2.4 *Loss assessment for sequences of cascading hazards scenarios*

We propose a simple economical consequence model that assigns the replacement cost ratios to every damage state of the building classes T_j^B. The incremental economic loss, defined as the difference in the expected loss resultant from the initial damage state and final damage state, is calculated in terms of the reference scheme B as:

$$p\left(L|D_{jw}^B\right) - p\left(L|D_{jz}^B\right) \quad \text{Eq. 10}$$

Combining the two inter-scheme compatibility matrices, ($p\left(T_k^A|T_j^B\right)$ and $\left(D_{kz}^A|D_{jy}^B\right)$, along with Eq. 7 and Eq. 10, we obtain the formulation in Eq. 11, which is identical to the one in Figure 1b. This allows us to calculate the probability of observing an incremental loss due to the cumulative damage during the sequence of hazard-scenarios.

$$p(L|IM^B \cap IM^A) = \sum_{k,y,z,w} p\left(T_k^A|T_j^B\right)p\left(D_{kz}^A|D_{jy}^B\right)p(D_{kz}^A|IM^A)p\left(D_{jw}^B|D_{jy}^B, IM^B\right)\left[p\left(L|D_{jw}^B\right) - p\left(L|D_{jz}^B\right)\right] \quad \text{Eq. 11}$$

Eq. 11 represents the disaggregated loss caused by the triggered event upon the buildings with a pre-existing damage (induced by IM^A). Finally, the likely loss for the entire sequence can be obtained by summing up Eq. 1 and Eq. 11.

3 Application example

3.1 *Context of the study area: Metropolitan Lima, Peru*

In 2022, Peru had a population of around 33 million people, with nearly 58% of this living in coastal communities. In Løvholt et al., (2014) it was stated that this country has the largest population exposed to tsunamis in the American continent. Lima, its capital, with nearly 10 million inhabitants (around one third of the country's population) is home to the most important political, industrial, and economic activities of the country. Lima ranks as the capital city exposed to the highest seismic hazard in South America (Petersen et al., 2018), and as the second city in the world in terms of the value of working days lost relative to the national economy due to earthquakes (Schelske et al., 2014). This city has suffered devastating disasters in the past. For instance, in 1586 and 1724 earthquakes triggered tsunami run-ups over 24 m (Kulikov et al., 2005). The 1746 earthquake, with an estimated magnitude of M_w 8.8 (Jimenez et al., 2013), produced a tsunami with local height of 15 to 20 m (Dorbath et al., 1990) and destroyed the city. In 1974, a M_w. 8.1 event produced widespread damage and caused losses of ~ 7.5 billion dollars. Since then, the city has been experiencing continuous urbanization with generally poor structural design (Tarque et al., 2019).

The 1746 earthquake for scenario for earthquake and tsunami modelling was also used in Adriano et al., (2014) to estimate the damage probabilities of the residential building stock of Callao (part of the Metropolitan area of Lima) using the empirical tsunami fragility functions of (Suppasri et al., 2013) for four building types. More recently, Ordaz et al., (2019) developed probabilistic earthquake and tsunami risk forecasts for Callao. However, that study did not describe the vulnerability models used, nor the method employed to address the non-linear damage accumulation. To the authors' best knowledge, neither

https://doi.org/10.5194/nhess-2022-183
Preprint. Discussion started: 6 July 2022

Natural Hazards and Earth System Sciences Discussions

cumulative damages due to earthquake and tsunami scenarios nor the use of analytical tsunami fragility functions for Lima have been reported in the scientific literature.

3.2 Scenarios of earthquake and tsunami for Lima

We use the dataset compiled by Gómez Zapata et al., (2021e) which is composed of six earthquakes with moment magnitudes ranging from 8.5 to 9.0 M_w, which were made available in Gómez Zapata et al., 2021c). In that dataset, each event is represented by an associated 1,000 realisations of cross-correlated ground motion fields (GMF) for peak ground acceleration (PGA) and spectral accelerations at 0.3 and 1.0 seconds. The selection of these spectral periods depends upon the fragility function's IM associated with the building classes of the exposure model (Sect. 3.3). The simulated GMF were obtained making use of the ground motion prediction equation (GMPE) proposed in Montalva et al., (2017) and the spatially cross-correlation model of Markhvida et al., (2018) employing the OpenQuake Engine (Pagani et al., 2014). For the site term of the GMPE, the dataset reported in Ceferino et al., (2018), which combined the slope-based Vs_{30} values of Allen and Wald, (2007) and a seismic microzonation (Aguilar et al., 2013) was used. On the tsunami modelling side, we reuse the data repository Harig and Rakowsky, (2021) that compiles tsunami inundations for each of the mentioned six earthquakes using the finite element model TsunAWI. Similarly as performed by Harig et al., (2020), the inundation values were interpolated to a raster file with grid cell dimensions of 10×10 m. Figure 4 shows three of the tsunami inundation scenarios for the study area.

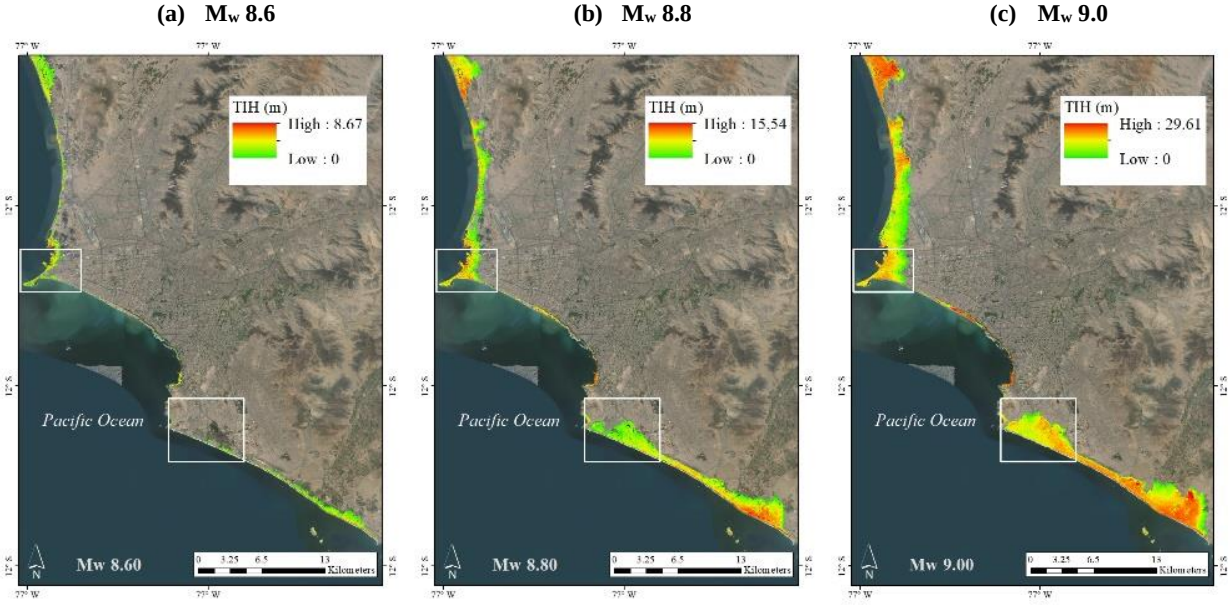

Figure 4. Expected tsunami inundation heights for three out of the six considered scenarios per moment magnitude (M_w). These raster products are available from Harig and Rakowsky, (2021). Two densely populated areas are depicted by white rectangles: in the north the "La Punta" (Callao) and Chorrillos in the south. Updated figure from Gómez Zapata et al., (2021e). Map data: ©Google Earth 2021.

https://doi.org/10.5194/nhess-2022-183
Preprint. Discussion started: 6 July 2022

Natural Hazards and Earth System Sciences Discussions

3.3 *Exposure modelling: taxonomic description, inter-scheme conversion and spatial aggregation of building classes for Lima*

We make use of the existing building exposure models that represent the residential building stock of Metropolitan Lima for ground shaking vulnerability that were developed by Gómez Zapata et al., (2021e) and are available from Gómez Zapata et al., (2021b). Such a building classification was defined by relating some covariates included within the last official Peruvian census from 2017 (INEI, 2017) at the block-level with respect to 21 classes proposed by the South American Risk Assessment (SARA) project (Yepes-Estrada et al., 2017) through a mapping scheme proposed from expert-elicitation (GEM, 2014). Since that information was provided for dwellings, the so-called "dwelling ratios" proposed by SARA were also implemented to obtain the building counts per class. A description of these building classes is presented in Table 1.

Table 1. SARA Building classes proposed for Metropolitan Lima and Callao with their replacement costs as reported in Yepes-Estrada et al., (2017). The intensity measures (IM) of their associated fragility functions, as reported in Villar-Vega et al., (2017), are also provided.

SARA building classes in Lima and Callao	Description	IM	Repl. Cost (USD/bdg)	Building counts
MUR-H1-3	Unreinforced masonry, between 1–3 stories	PGA	18,000	248799
MUR-ADO-H1-2	Unreinforced masonry (MUR) with adobe (ADO), 1–2 stories	PGA	15,000	209837
MUR-STDRE-H1-2	Dressed stone (STDRE) unreinforced masonry, 1–2 stories	PGA	15,000	209837
W-WBB-H1	Wood (W), bamboo (WBB), 1 story	S.A at 0.3s	12,000	187355
W-WWD-H1-2	Wood, bahareque and Quincha (WWD, wattle and daub construction), 1–2 stories	S.A at 0.3s	15,000	149884
W-WS-H1-2	Wood, solid wood (WS), 1–2 stories	S.A at 0.3s	12,000	127401
W-WLI-H1-3	Wood (W), light wood (WLI), 1–3 stories	S.A at 0.3s	31,500	123654
ER-ETR-H1-2	Reinforced (ETR) rammed earth (ER), 1–2 stories	PGA	15,000	89931
MUR-STRUB-H1-2	Unreinforced masonry with rubble (field stone) or semi-dressed stone, 1–2 stories	PGA	15,000	89931
W-WHE-H1-3	Wood, Heavy wood (WHE), 1–3 stories	S.A at 0.3s	12,000	82436
MCF-DNO-H1-3	Confined masonry (MCF), non-ductile, 1–3 stories	PGA	40,500	66749
MCF-DUC-H1-3	Confined masonry, ductile, 1–3 stories	PGA	126,000	66749
MR-DUC-H1-3	Reinforced masonry, ductile, 1–3 stories	PGA	360,000	16745
CR-LFINF-DNO-H1-3	RC with infilled frame, low rise (non-ductile)	PGA	126,000	13925
UNK	Unknown	S.A at 0.3s	12,000	8432
CR-LFINF-DUC-H1-3	RC with infilled frame, low rise (ductile)	PGA	288,000	7519
CR-LDUAL-DUC-H4-7	Reinforced concrete (RC) with dual wall system, medium rise (ductile)	S.A at 1.0s	1,080,000	125
CR-LWAL-DNO-H4-7	RC wall system, non-ductile, 4–7 stories	S.A at 1.0s	472,500	76
CR-LWAL-DUC-H4-7	RC wall system, ductile, 4–7 stories	S.A at 1.0s	1,080,000	76
CR-LWAL-DUC-H8-19	RC wall system, ductile, 8–19 stories	S.A at 1.0s	3,456,000	34
CR-LDUAL-DUC-H8-19	RC with dual wall system, high rise (ductile)	S.A at 1.0s	3,456,000	32

https://doi.org/10.5194/nhess-2022-183
Preprint. Discussion started: 6 July 2022

Natural Hazards and Earth System Sciences
Discussions

It is worth noting that although these typologies are similar to those of the SARA exposure model, there are differences between the building counts reported by that project and our model. This might be due to the vintage of the input census datasets (2007 vs. 2017, respectively), the thematic detail induced by the spatial aggregation entities (districts/ blocks/ CVT), having merged some building classes in terms of similar heights, and having reduced the number of unknown (UNK) type (~91% with respect the SARA model). The resultant exposure model is made up of ~1,657,635 residential buildings, a 25% increase with respect the SAA model. However, as observed in Gómez Zapata et al., (2022b), this scheme does not properly capture the presence of high-rise buildings, underestimating their presence while overestimating the wooden types.

These SARA buildings are spatially aggregated onto Central Voronoi Tessellations (CVT) to form seismic-oriented exposure models. It is worth noting that the construction of such heterogeneous aggregation units was based on the selection of an underlying distribution that spatially combined and normalised two weighted map layers, namely: (1) a tsunami inundation depth from a Mw 9.0 scenario (70% weight), and (2) the population density at the block level (30%). The resulting model provides higher resolution cells where both conditions are maximised whilst coarser geocells occur when one can expect their absence. Further details about these models are available in Gómez Zapata et al., (2021a, b). Figure 5 shows the percentage of building typologies grouped by their main structural materials expected within each geocell.

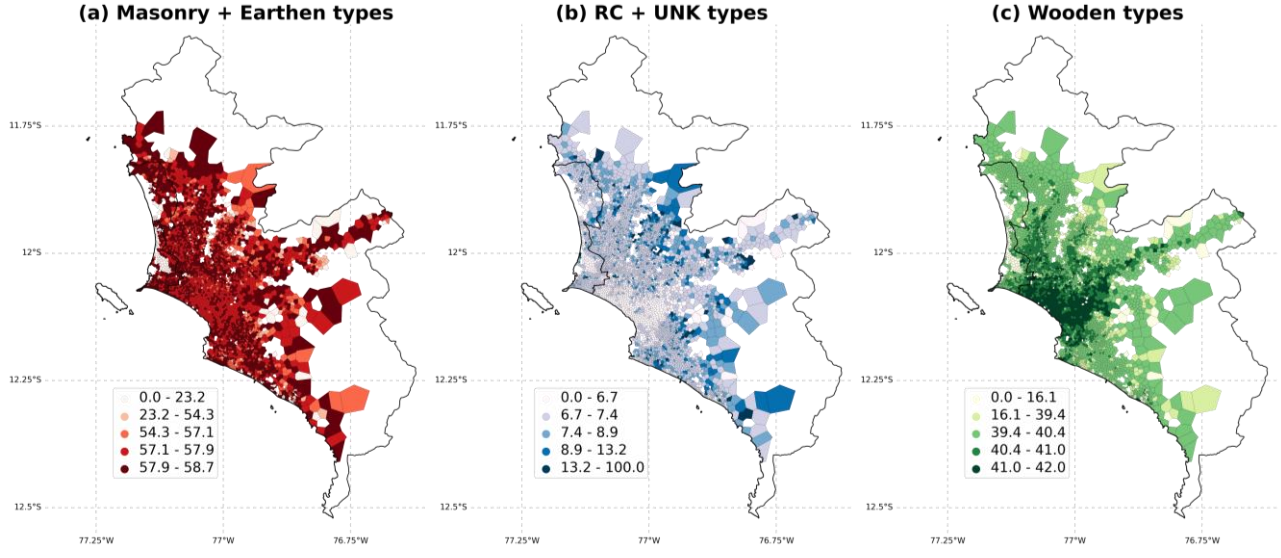

Figure 5. Spatial distribution of the percentage of the main structural material of the residential buildings in Metropolitan Lima in each CVT geocell using the dataset of Gómez Zapata et al., (2021b). The colour scale represents the material type (red: masonry and earthen; blue: reinforced concrete and UNK; green: wooden types). Only CVT that intersected the census-based blocks (INEI, 2017) are shown.

The analytically derived set of seismic fragility functions by Villar-Vega et al., (2017) are assigned to every SARA class. They will be used to obtain the damage distribution for the cross-correlated ground motions per earthquake scenario (Sect. 3.2). For this vulnerability assessment, we use the replacement cost as given by Yepes-Estrada et al., (2017a), presented in Table 1. For their damage states, we assumed loss ratios of 2%, 10%, 50%, and 100%, respectively.

https://doi.org/10.5194/nhess-2022-183
Preprint. Discussion started: 6 July 2022


Natural Hazards and Earth System Sciences Discussions

On the tsunami vulnerability side, we represent the commonly exposed residential building stock to earthquakes and tsunamis in terms of two classification schemes, namely the Suppasri et al., (2013) and Medina, (2019) schemes which provide sets of empirical and analytical fragility curves, respectively. The former one was made available for Lima in Gómez Zapata et al., (2021b) and is comprised of six typologies. Notably, its corresponding set of empirical tsunami fragility functions (with six damage states) was derived by implicitly addressing the damage induced by the ground-shaking after the M_w 9.1 2011 Japan earthquake and tsunami. Due to this reason, the steps outlined in Sections 2.2 and 2.3 are not developed for the Suppasri et al. (2013) scheme. Their related direct scenario-based loss estimates were reported in Gómez Zapata et al., (2021e) from the variations obtained from seven geographical entities used to spatially aggregate the residential building portfolio of Lima, and presented in Sect. 4 for comparative purposes in contrast with the offered method applied to the Medina (2019) scheme. This second type of classification is to the authors' knowledge the only available model that provides analytical far-field tsunami fragility functions for the South American Pacific Coast. It includes six typical buildings located in Tumaco (Colombia) initially defined in Medina, (2019), which are generalized in this study. They are M-PN (wooden), M-MP (masonry), M-PCP1-T1 (framed RC, one storey with similar length-width ratio), M-PCP1-T2 (framed RC, one storey, with a higher length to width ratio), M-PCP2 (framed RC, 2 storeys), and M-PCP3 (framed RC, 3 or more storeys). Their associated set of fragility functions was developed following the method proposed in Medina et al., (2019) to define the structural fragility due to tsunami forces. A summary that regards the structural characteristics of these building types and the method adopted in deriving these models are provided in the data repository Gómez Zapata et al., (2022a).

As explained in Sect. 2.1, every building class within the three schemes of interest is disaggregated into attributes within the GEM v.2.0 faceted taxonomy. As done in Gómez Zapata et al., (2022b), fuzzy compatibility levels between the attribute values and building classes are assigned through expert elicitation. Thereby, synthetic surveys based on the possible combinations of attributes that every building class may describe are employed to solve the compatibility scores and obtain the probabilistic inter-scheme compatibility matrices in the form of $p\left(T_k^A \middle| T_j^B\right)$. Subsequently, we can obtain the building counts under the tsunami classification scheme. This is done considering the SARA classification (Figure 6a), as the source scheme $\{R\}_{T_k^A}$ and the inter-scheme conversion matrix (Figure 6b). Then, the corresponding counts under the tsunami scheme of Medina (2019) $\{R\}_{T_j^B}$ (Figure 6c) are obtained by applying a dot product (Eq. 2).

The inter-scheme conversion between SARA and the Suppasri et al., (2013) classes for Lima was reported in Gómez Zapata et al., (2021e). The replacement costs values of the building classes within the Medina (2019) scheme are assumed to be the same as the SARA class for which the largest compatibility value was obtained from the inter-scheme compatibility matrix (Figure 6-b). We have adopted identical loss ratios per limit damage state as the ones assumed for earthquake vulnerability. Similar loss ratios were also adopted in Antoncecchi et al., (2020) to assess the vulnerability of buildings to tsunamis using empirical fragility functions. It is worth noting that only the commonly exposed buildings to each pair of hazard scenarios (i.e., intersection between the IM of Figure 4 and Figure 5) are considered for the assessment of cumulative damage after the cascading sequence.

https://doi.org/10.5194/nhess-2022-183
Preprint. Discussion started: 6 July 2022

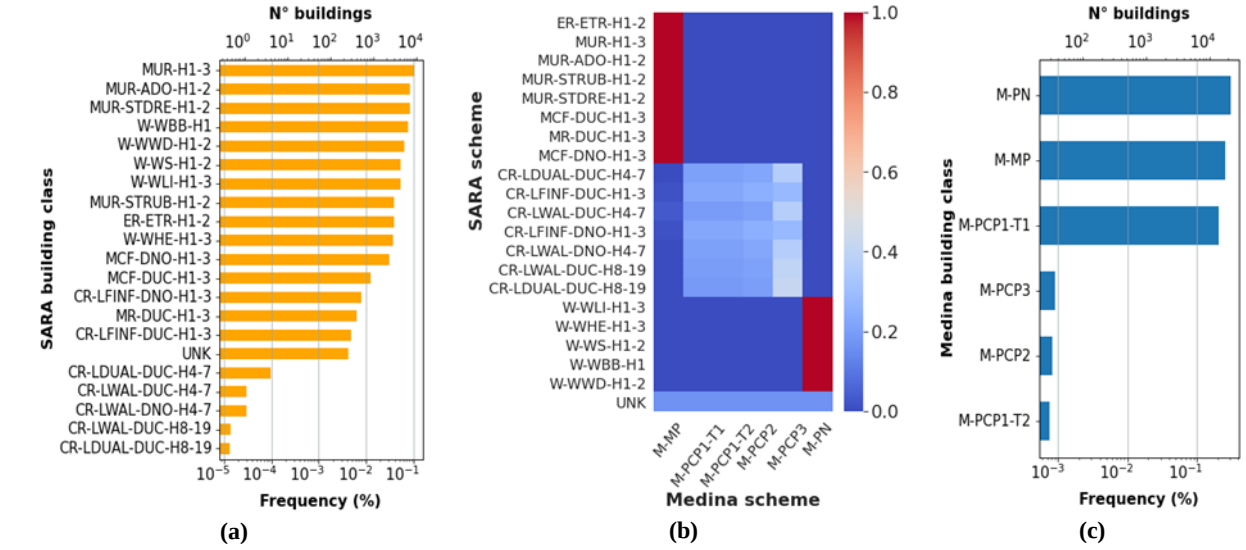

Figure 6. Classification of the buildings in the maximum exposed area to both perils (M_w 9.0 scenario) in terms of the (a) seismic-vulnerability oriented SARA classes (used as a source scheme) and (b) the inter-scheme conversion matrix. The former two models are used as inputs to obtain the (c) proportions for the tsunami-oriented building classes of Medina (2019).

3.4 *The probabilistic description and compatibility of inter-scheme damage states for Lima*

We obtain the inter-scheme damage compatibility matrices, $p\left(D_{kz}^{A}\middle|D_{jy}^{B}\right)$, following the method presented in Sect. 2.2 to probabilistically harmonise the damage states that define the fragility functions of *A* (SARA) and *B* (Medina). It is worth noting that although *A* and *B* comprise four damage states they do not have a trivial equivalence. *A* defines a single damage criterion for the entire set of building classes closely following the proposal by Lagomarsino and Giovinazzi, (2006) as a function of the yielding and ultimate spectral displacements. Conversely, *B* uses a building class-dependent parametrization based on the HAZUS inter-storey drift ratios to define the structural damage levels on pre-code structures.

First, we use the AeDES scale to score the admissible observable damage extension on individual building components (n in Eq. 3) through expert elicitation, which can jointly describe each building-specific damage states of every scheme's fragility functions (D_{kz}^{A}, D_{jy}^{B}). Some examples of this procedure are displayed in Figure 7. These heuristics configure the training datasets. Subsequently, we have configured the testing datasets. They are composed of a synthetic dataset of 10,000 exhaustive possible combinations of the observable AeDES score-based damage extension $\{OD\}_n$. Thereby, the likelihood terms and $p\left(D_{jy}^{B}|\{OD\}_n\right)$ in Eq. 6 represent the probability of classifying each damage state D_{kz}^{A} and D_{jy}^{B} given the set of scored building components $\{OD\}_n$.

https://doi.org/10.5194/nhess-2022-183
Preprint. Discussion started: 6 July 2022

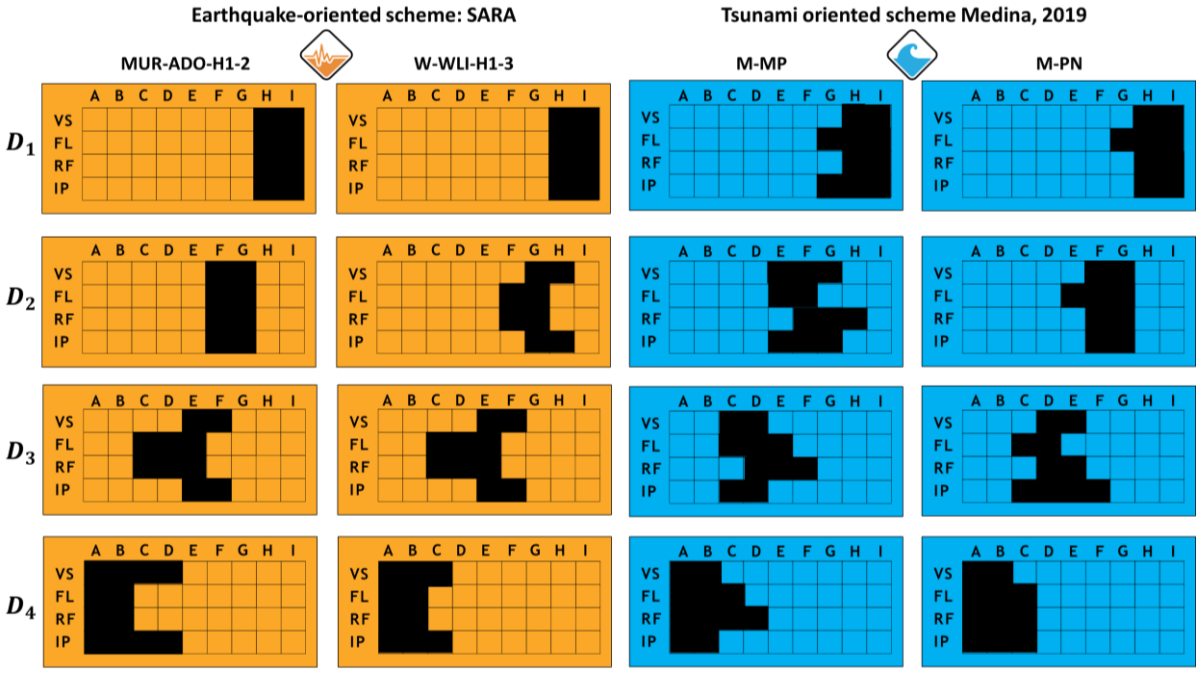

Figure 7. Examples of the AeDES-based heuristics (see Figure 2 and Eq. 3) used to describe the expected observable damage features per damage state per building class within two hazard-dependent vulnerability schemes.

To obtain the likelihood terms of in Eq. 6, we have decided to use the Gaussian Naïve Bayes supervised machine-learning classification-algorithm. It is available in the free software library Scikit-learn for the Python programming language (Buitinck et al., 2013). This selection is suitable for our classification problem because the observable damage heuristics can be assumed as normally distributed continuous data. This can be observed from the heuristic shown in Figure 7 where the central damage states (i.e., moderate and extensive) show wider ranges of combinations of observable damage with respect to the lowest (slight) and largest (collapse) states. For illustrative purposes, in Figure 8 we show one of the possible sets for the likelihood probabilities predicted for each damage state described in terms of observable damage extension with respect to the AeDES scale upon two building components (VS, IP) for two material-based typologies in the commonly exposed area to both perils, i.e., masonry and wooden structures (see Figure 6a,c).

The marginal probability in Eq. 6, $p(\{OD\}_n)$, is assumed to be the proportion between one observation and the exhaustive combinations (1/10,000). Thereafter, we have obtained the probabilistic inter-scheme damage matrix $p\left(D_{kz}^{A}|D_{jy}^{B}\right)$ for each combination of building types from the two schemas (i.e., 21 SARA classes by 6 Medina classes = 126 conversion matrices). Examples of the inter-scheme damage matrices are shown in Figure 9 for three pairs of building types that had the highest inter-scheme compatibility values in Figure 6b. Each of the 126 matrices that relates the damage states for each possible combination of building classes from the two schemas is subsequently weighted by the corresponding value of $p\left(T_k^A|T_j^B\right)$, that is, by the probability of the building classes of the two schemas actually being descriptive of the same actual building (i.e.,

https://doi.org/10.5194/nhess-2022-183
Preprint. Discussion started: 6 July 2022

Natural Hazards and Earth System Sciences
Discussions

Figure 6-b). When considered in Eq. 11, the damage related matrices are maximized by the most compatible pairs of inter-schema building matrices. The scripts, heuristics, the final set of likelihood distributions, and the related set of compatibility matrices are provided in Gómez Zapata et al., (2022c).

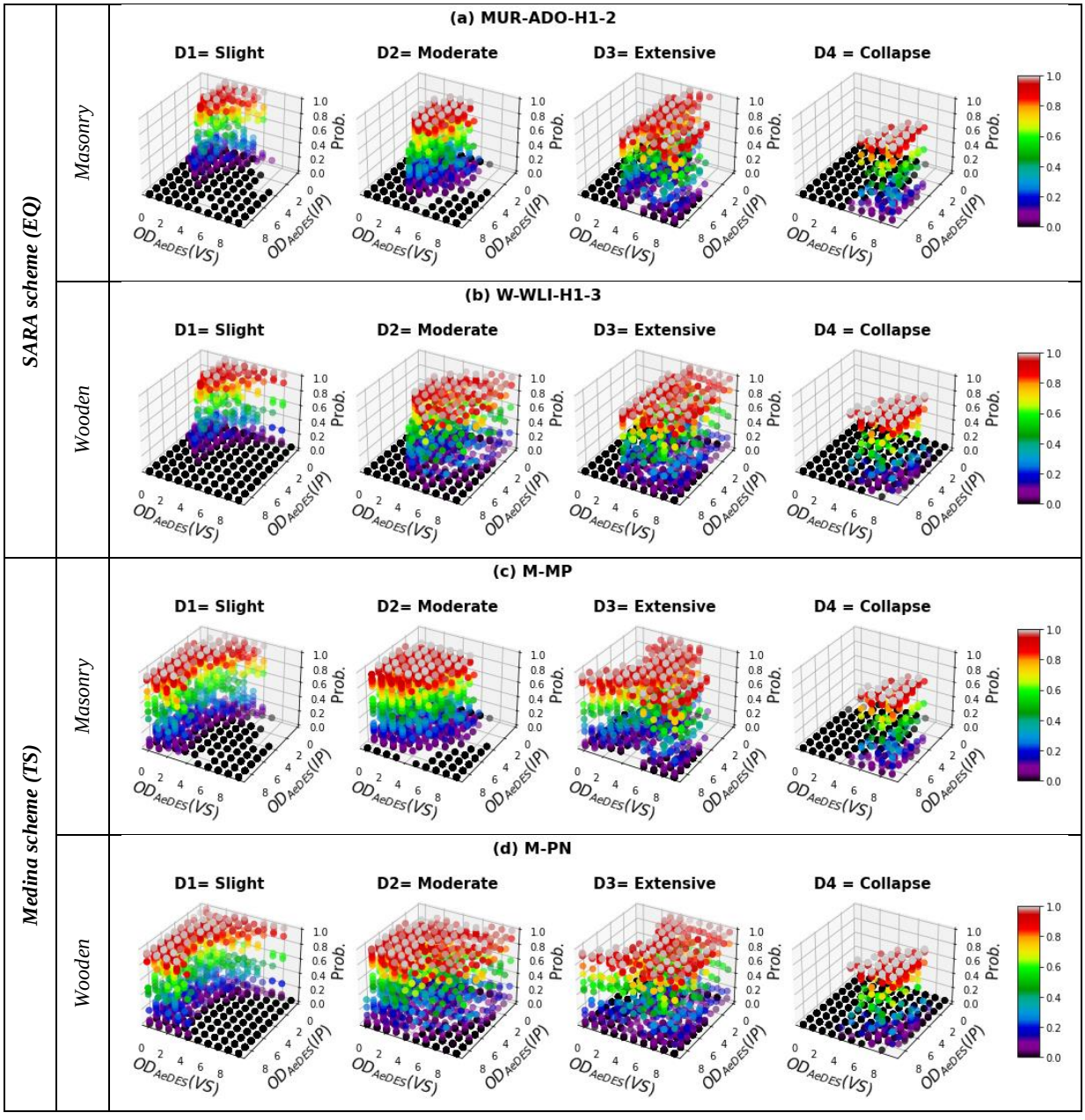

Figure 8. Predicted likelihood probabilities of classifying each damage state D_{jz}^{A} (SARA classes) and D_{ky}^{B} (Medina classes) given the combinations of observable damage$\{OD\}_n$ in terms of the AeDES scale for mansonry (a, c) and wooden (b, d) buildings.

https://doi.org/10.5194/nhess-2022-183
Preprint. Discussion started: 6 July 2022

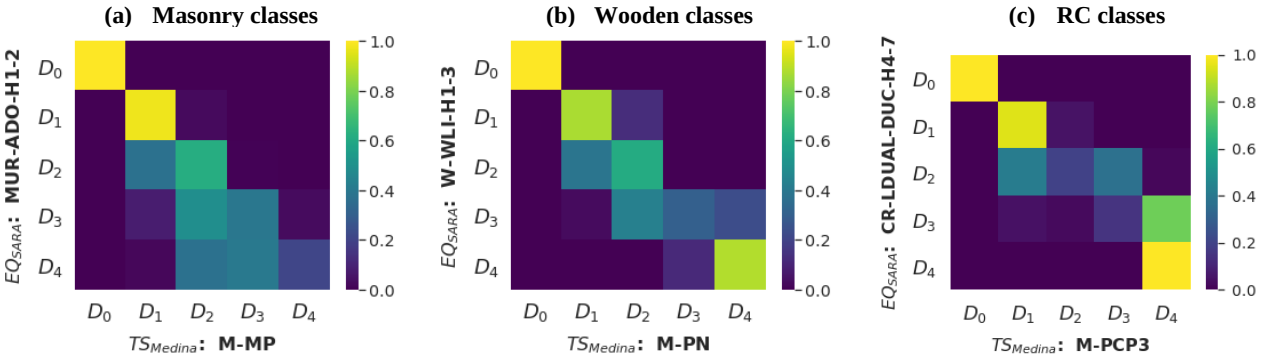

Figure 9. Probabilistic inter-scheme damage compatibility matrices for three pairs of building classes whose fragility functions are comprised within the source (D_{kz}^{A} SARA (EQ: earthquake-oriented) and the target $\left(D_{jy}^{B}\right)$ Medina (TS: Tsunami-oriented) vulnerability schemes.

3.5 Tsunami state-dependent fragility functions for Lima

We have followed the method presented in section 2.3 to configure the state-dependent fragility functions based on Scheme *B* (Medina) with associated analytical far-field tsunami fragility functions. The parameters that define the lognormal cumulative distributions for the four original damage states (assuming an initial undamaged state), and well as for the set of $G_f = 10$ transitions probabilities (from Eq. 8) are provided in the data repository Gómez Zapata et al., (2022a). Figure 10 shows the analytical tsunami fragility functions (continuous lines) and state-dependent fragility curves with their respective damage-transitions (non-continuous lines) for the six building classes.

From Figure 10 it is possible to observe some features of the tsunami damage-state fragility functions based on ad-hoc calibration parameters (Sect. 2.3). For example, the masonry buildings class is the one most fragile to tsunami forces when in an undamaged state. Consequently, their associated state-dependent fragilities are shifted towards the left side of the plot in quite an extreme fashion (Figure 10-a). This means that for that building type there is a higher probability for it to follow a longer damage progression after having been strongly affected by the seismic ground-shaking (dotted and dashed lines). Conversely, for the wooden buildings (Figure 10-b) these are more likely to follow a damage progression than other classes if they were slightly affected by the shaking (see dashed lines). For the two one-storey RC building types assessed (M-PCP1-T1 & M-PCP1-T2) there are negligible differences between the transition probabilities D_2-D_3 and D_3-D_4, as well as between D_1-D_3 and D_2-D_4. Notably, the inter-distances between these pairs of sets (of damage states) are of a similar order as the ones comprised by one and two damage state(s) respectively. This feature is not present for the other RC buildings with increasing heights nor the wooden types. This observation is dependent on the specific analytical fragility models used and the assumptions adopted to derive them (Eq. 10) and no generalization should be done until it can be further validated through other means.

https://doi.org/10.5194/nhess-2022-183
Preprint. Discussion started: 6 July 2022

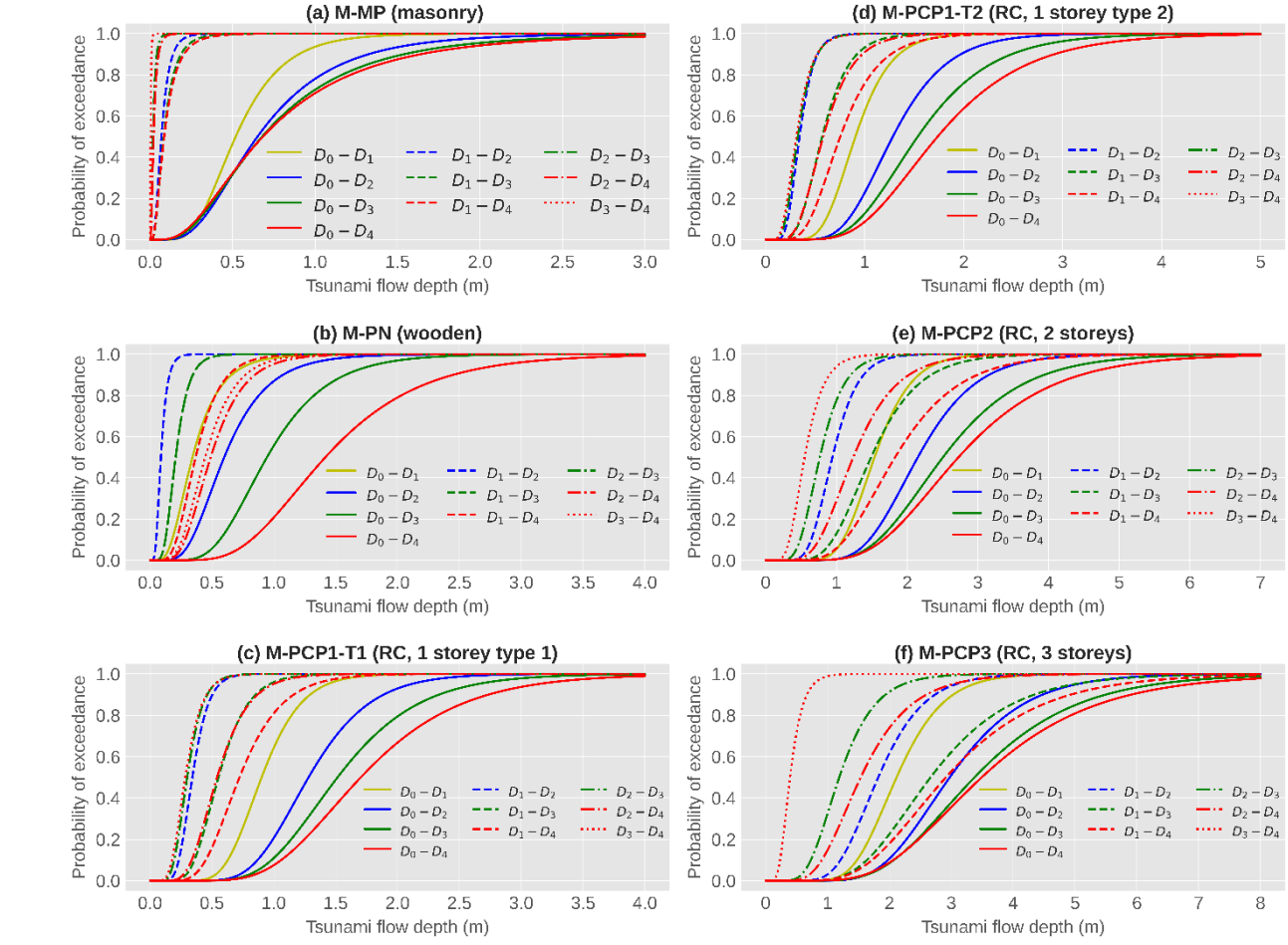

Figure 10. Analytical tsunami fragility functions with initial undamaged state as proposed by Medina, (2019) (continuous lines) and derived state-dependent fragility curves (non-continuous lines) for six building classes in terms of flow depth (m) as IM.

3.6 Cumulative damage from consecutive ground shaking and tsunami scenarios in Lima

The spatially cross-correlated ground motion fields (Sect. 3.2, Fig. 11-a, b), along with the exposure model for seismic vulnerability and their corresponding fragility functions (Sect. 3.3, Fig. 11-d, e) are the first set of inputs required by the engine DEUS (Brinckmann et al., 2021) to estimate the damage distribution and direct economic losses for the residential building stock of Lima after each earthquake scenario. DEUS is a software designed to compute scenario-based risk from any type of natural hazard over spatially aggregated building portfolios. This version of DEUS is an open-source Python program whose number of executions are proportional to the consecutive risk scenarios.

As shown in f, g, the resulting damaged exposure model (after ground-shaking) is used as input for a second execution to account for the cumulative damage induced by the tsunami scenarios. DEUS makes use of the two sets of inter-scheme

https://doi.org/10.5194/nhess-2022-183
Preprint. Discussion started: 6 July 2022

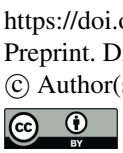

Natural Hazards and Earth System Sciences
Discussions

compatibility matrices for buildings (Sect. 3.3) and damage states (Sect.3.4) to change from the source earthquake reference scheme to the target tsunami reference scheme (see Fig. 11-g). These are inputs together with the tsunami inundation heights (Sect. 3.2, Fig. 11--c), and state-dependent tsunami fragility functions (Sect. 3.5, Fig. 11-h) for the second run of DEUS. This time, the damage states are updated in the building exposure model, delivering only the disaggregated damage and losses expected from the tsunami. Finally, the cumulative distribution of losses is obtained by adding the latter disaggregated tsunami losses with the initial results derived from the earthquake ground-shaking.

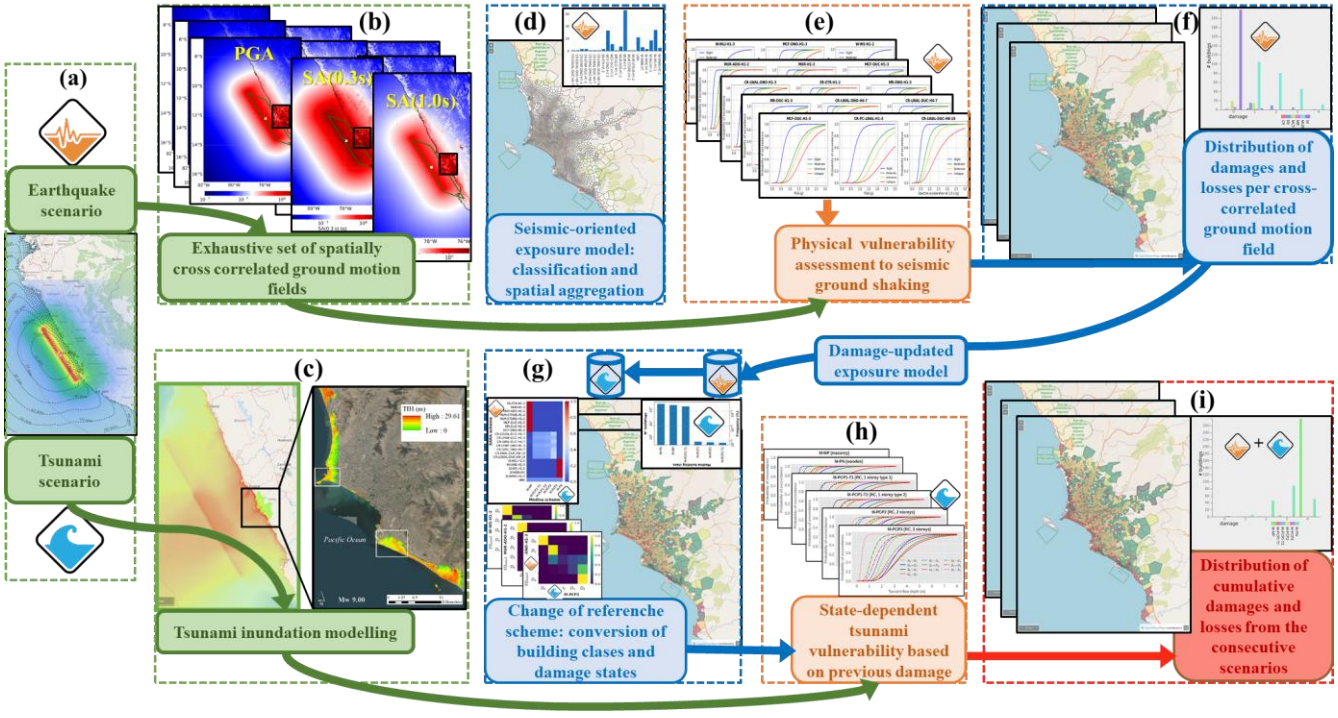

Figure 11. Proposed workflow for multi-risk assessment in Lima from each pair of consecutive earthquake and tsunami scenarios. A M_w 8.8 event is displayed as an example. The processes regarding the natural hazardous events are highlighted in green. Blue and orange indicate the exposure and vulnerability processes, respectively. The spatially cross-correlated ground motion fields and an initial exposure model (with earthquake-oriented classes) are input for the seismic vulnerability process, which provides the damage-updated exposure models. After the reference scheme conversion processes (building classes and damage states), these sets of damaged-exposure models are inputs for the state-dependent tsunami fragility functions to finally obtain the distribution of cumulative damages and losses (red). Map data of subplot (c) is from ©Google Earth 2021.The basemap and data of suplots (d), (f), (g), (i) are from © OpenStreetMap contributors 2021. Distributed under the Open Data Commons Open Database License (ODbL) v1.0)

4 Results

The generated results are presented in the form of loss exceedance curves in Figure 12. This figure reports the probability of exceeding the selected loss metric (replacement cost in USD) for the six earthquake and tsunami scenarios that might impact the portion of the residential building stock of Lima that is commonly exposed to each pair of hazard scenarios. This figure shows five sets of curves, hereby described:

https://doi.org/10.5194/nhess-2022-183
Preprint. Discussion started: 6 July 2022

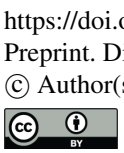

Natural Hazards and Earth System Sciences
Discussions

1. Earthquake ground-shaking-induced loss (blue curves). They represent the direct losses due only to seismic ground shaking using the SARA scheme (Villar-Vega et al., 2017). They are obtained through 1,000 realisations of cross-correlated seismic ground motion fields using the models described in section 3.2.
2. Losses obtained from the sole use of empirical fragility functions as simulating a near field tsunami (red curves). These curves represent the losses from the cumulative effects of the shaking and the tsunami (without any possibility to separate both effects). Such losses prediction may be biased since the empirical fragility functions of (Suppasri et al., 2013) assuming an initial undamaged state (D_{k0}^{A}) has not been validated for smaller or larger events. Similarly as it was concluded in Gómez Zapata et al., (2021), we have also observed that as the earthquake magnitude increases, the differences between the two largest loss values in the curve (from the two finest resolution entities) are reduced.

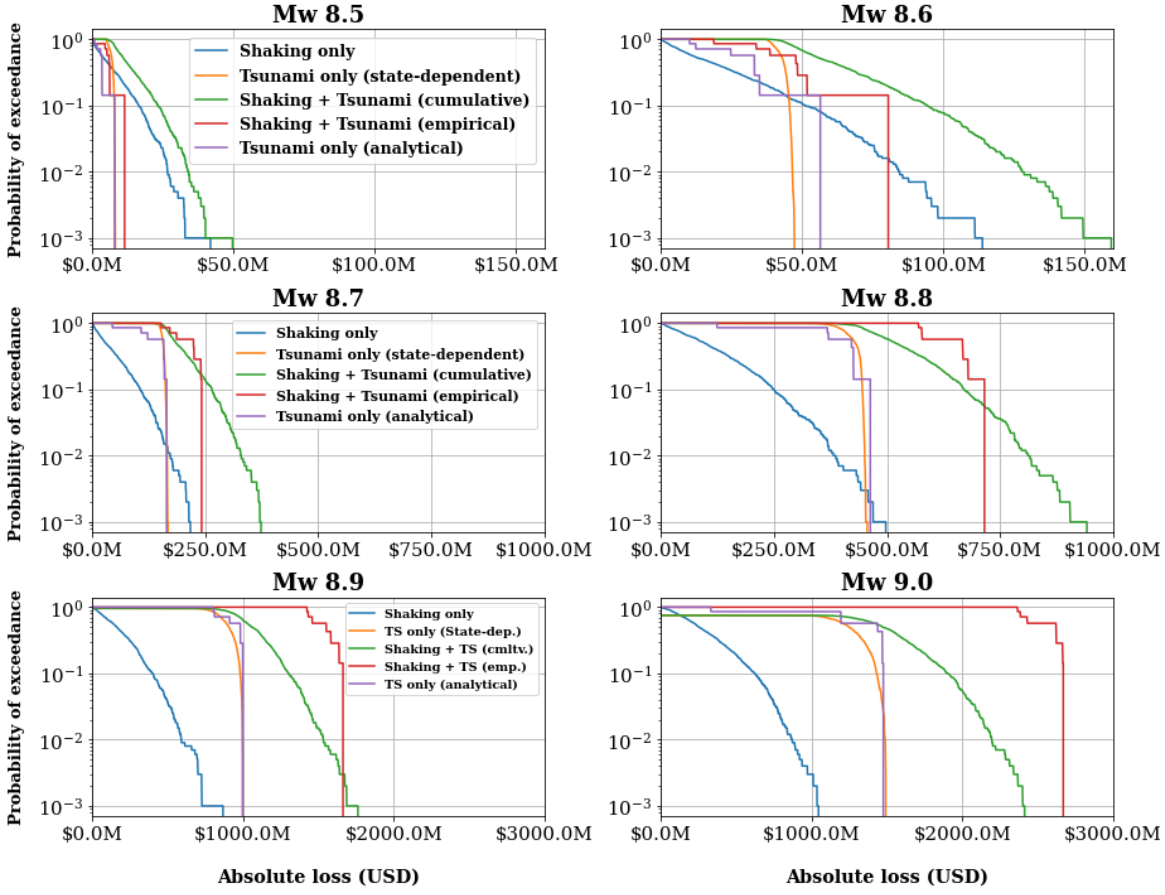

Figure 12. Five loss exceedance curves for the residential building portfolio of Lima are presented in each subplot per earthquake magnitude scenario (M_w 8.5-9.0). Three out of the five curves represent the disaggregated losses per hazard event: shaking-induced losses only (blue); far-field tsunami-induced losses (initial undamaged state, purple); state-dependent tsunami-induced losses (with pre-existing shaking induced damage, orange). The green curves represent the losses expected from the cascading sequence whilst the red ones show the losses derived solely using empirical tsunami fragility functions.

https://doi.org/10.5194/nhess-2022-183
Preprint. Discussion started: 6 July 2022


Natural Hazards and Earth System Sciences Discussions

3. Losses obtained from the sole use of analytical fragility functions as simulating a far-field tsunami (purple curves. They represent the direct losses obtained solely through the implementation of the analytical tsunami fragility tsunami Medina, (2019), while assuming an initial undamaged state (D^A_{k0}), thus, neglecting seismic ground-shaking. Similarly, as done for the former case (empirical functions), the reduced variability of these results was accounted for through computations using seven exposure models, with variable spatial resolutions obtained from a recent study (Gómez Zapata et al., 2021e). This is a result of the lack of variability in the seismogenic parameters to vary only the M_w, and not having assumed distributions for slip-rates, but single values.
4. The losses related to the tsunami event obtained after using our method (state-dependent fragility functions, orange curves). They represent the direct losses which were only derived from the updated exposure model (i.e., with non-zero damage states)). This means that these curves only represent the tsunami-induced losses for buildings that have already experienced earthquake-related damage. These loss exceedance curves are constructed using Eq. 11. Thus, this procedure implied the inter-scheme building conversion $p\left(T^A_k \middle| T^B_j\right)$ derived in section 3.3, the inter-scheme damage state conversion $p\left(D^A_{kz} \middle| D^B_{jy}\right)$ obtained in Sect. 3.4, as well as the state-dependent tsunami fragility functions constrained in Sect. 3.5.
5. Cumulative losses (our method) induced by the ground-shaking and tsunami sequence (green curves). They represent the losses obtained by adding the shaking-induced losses (blue curves) with the aforementioned disaggregated tsunami-induced losses (orange curves), that is, the outcome of the method proposed in this paper. These green curves represent, according to our approach, the likely losses that would be expected from each magnitude-dependent scenario-based cascading sequence over the considered building stock.

Hereafter we describe some observations that arise from Figure 12.

1. The resultant losses obtained after having used the two sets (empirical or analytical) of tsunami fragility functions (while assuming initial undamaged states) are profoundly different. As expected, the use of the empirical tsunami fragility model (red curves) is, for all the magnitudes, leads to larger values in comparison with the values obtained from the analytically derived fragility functions (purple). These differences increase with magnitude. This feature might arise, not only from the fact that empirical fragility functions consider both earthquake and tsunami actions while the purple curves consider only the effects of the tsunami, but also because empirical fragility functions only account for flow depth as the IM. Conversely, the analytical fragility functions implemented were derived using the theoretical forces associated with the flow velocity tsunami waves as input in the generating numerical model. Similar observations regarding the reduction in the loss estimations when flow velocity is included have been drawn by other studies (e.g., Attary et al., 2019; Park et al., 2017).
2. We observe that the ground-shaking dominates the losses at lower magnitudes (Mw 8.5, 8.6), whilst the tsunami, either from analytical (emulating far-field tsunamis) or empirical fragility functions (near-field tsunamis), controls the losses for the rest of the scenarios with larger magnitudes. The former is aligned with the observations of Goda

https://doi.org/10.5194/nhess-2022-183
Preprint. Discussion started: 6 July 2022

and De Risi, (2018) and Gómez Zapata et al., (2021e) for the case of empirical tsunami models. Moreover, a similar trend is observed for the disaggregated tsunami-induced losses (assuming initial non-zero damage) whose respective loss values (orange curves) are larger than the shaking-induced losses for M_w 8.8, 8.9, and 9.0. Hence, these features highlight that as the magnitude increases, there is an increasing comparative importance of the tsunami risk within the considered sequence of hazards.

3. Expected loss values from cumulative damages based on single-hazard vulnerability models (our method, green curves) are clearly different from the one produced by classical empirical tsunami models. Classical empirical tsunami fragility functions lead to considerable lower losses estimations for the low magnitudes earthquakes and substantial larger estimations for the larger ones.
4. The differences between the loss exceedance curves derived from both sets of analytical fragility models (either from undamaged or with pre-existing damage) are larger for the lower magnitudes (M_w 8.5, 8.6) and decrease with increasing magnitude. As the magnitude increases, there is an increasing tendency of convergence between these two loss curves (M_w 8.9, 9.0).
5. Consequently, since tsunami-induced losses either from analytical fragilities (initial undamaged states) or from state-dependent and inter-scheme models converge for the larger magnitudes (M_w 8.9, 9.0), their respective summations with the shaking-induced losses would be approximately similar at the largest probabilities of exceedance. Nevertheless, this observation needs to be better investigated through more exhaustive simulations of tsunami inundation per considered scenario.
6. Conversely, considering observation 3, (i.e., as the magnitude decreases, the differences between purple curves and orange curves increases), their respective summations with the shaking-induced losses will lead to very different results. Hence, this observation suggests that, although earthquake and tsunami structural responses can be separately approximated for very large magnitudes, it is still required to address cumulative damages from the vulnerability interactions that are expected on the lower magnitudes earthquakes we have considered (i.e., M_w. 8.5, 8.6).

When we consider analytical fragility functions with D_{k0}^{A} that only emulate the damaging actions of far-field tsunamis (without any ground shaking), we observe that as the magnitude increases, their respective loss exceedance curves converge with the ones that assumed state-dependency (D_{kz}^{A}). This is because, for the larger magnitude events, the damaging actions due to seismic ground shaking will correspondingly increase. Hence, the available probabilistic damage transitions from the damage states within the earthquake (source) to tsunami (target) schemes will be consequently reduced. Therefore, we observe that if far-field analytical tsunami fragility functions are used, their corresponding results will be very much alike, regardless of whether they are considered as being undamaged (D_{k0}^{A}) or with pre-existing damage (D_{kz}^{A}). Therefore, for these larger magnitude events, regardless of which curve is summed up with the shaking-induced losses, the resulting loss distributions for the hazard sequence would lead to quite similar results. Thus, the implementation of state-dependency on tsunami fragility may not be fully necessary to be addressed for very large earthquake magnitudes (M_w 8.9, 9.0). This observation is aligned

https://doi.org/10.5194/nhess-2022-183
Preprint. Discussion started: 6 July 2022

with studies (i.e., (Petrone et al., 2020; Rossetto et al., 2018)) that suggest that earthquake and tsunami structural responses can be separately approximated. However, the former statement would not apply to the low magnitude earthquakes investigated in Lima for which the pre-existing damage due to earthquakes must be addressed. No generalizations should therefore be done in this regard, with sensitivity analyses needing to be carried out in the future.

5 Discussion

This study has proposed a modular method to disaggregate the direct losses expected for building portfolios exposed to consecutive hazardous scenarios of different natures in which their individual components could be individually improved. Therefore, future sensitivity analyses on some of the modules related to damage-state would benefit the understanding of how their embedded uncertainties would impact their corresponding results. We can mention:

1. The disaggregation of building classes into taxonomic attributes as presented in Sect. 2.1 is an important input to obtain the probabilistic inter-scheme building compatibility matrices based on Gómez Zapata et al., (2022b). However, it is worth noting the shortcoming described by Charvet et al., (2017) referring to the generalised poor taxonomic building characterizations of the currently available tsunami fragility models. They are, most of the time, only based on their main construction material, although sometimes they include the number of storeys, and rarely do they include other attributes such as the date of construction (e.g., Suppasri et al., (2015). When more enriched descriptions for tsunami vulnerability get available in the future, this approach will remain useful for similar purposes.
2. When/if local high quality empirical data collection and analytical models), become available, they could be used to constrain the relationships between the failure mechanisms and attribute relevance for hazard-related susceptibilities. This might contribute to enhance the construction of heuristics that characterise the likely observable damage extent (per damage limit state, building type and hazard-dependent fragility model), that could be obtained through more refined approaches such as unsupervised machine learning. Its use applied on real datasets that document observations on building components (even different from the ones presented in Eq. 3) could contribute to refine state-dependent tsunami fragility functions and to restrict the heuristics on the likely observable damage (Sect. 2.2) and thus, minimizing subjective expert judgment. In this sense, it is worth noting that the set of predicted likelihood probabilities in the probabilistic compatibility degree between damage states from different hazard fragility functions that we derived from the synthetic datasets created through the heuristics and the AeDES scoring system are not unique, as they depend on the choice of machine learning technique and on the heuristics derived through expert elicitation. In this sense, we have documented a preliminary sensitivity analysis on such parametrization in Gómez Zapata et al., (2022c). However, further investigation of the impact of such parametrization is still advised.

https://doi.org/10.5194/nhess-2022-183
Preprint. Discussion started: 6 July 2022


Natural Hazards and Earth System Sciences Discussions

3. As described by Hill and Rossetto, (2008), we have observed that, when characterising damage states due to the impacts of natural hazards on buildings, there is still the need for standardisation in describing observable physical damage after any kind of hazardous event through the harmonisation of damage scales for data collection, not only on entire building units but also regarding the particular damage (and extent) experienced by certain individual components. In this regard, although we have used the AeDES scale, other damage scales could be more suitable to describe the observable damage to some building classes than for others (Hill and Rossetto, 2008; Turchi et al., 2022). Nonetheless, the choice of a standard scale to transversally describe any observable set of damage on buildings will benefit the research in multi-hazard vulnerabilities.
4. The integration of economic consequence models for physical vulnerability based on the replacement costs as a function of the buildings' area, as for instance presented in Triantafyllou et al., (2019) for tsunami vulnerability is worth testing. This also depend on the available data and it is out of the scope of this paper, but it would be worth exploring their contribution once more refined estimations about replacement cost are available for Lima. Nevertheless, one should be aware on the uncertainties involved for large scale building exposure models.

The derivation of the hazard intensities could also benefit from future enhancements. For instance, the GMPE-based seismic accelerations derived on a simplified Vs_{30} site-grid of ~1 km might be too coarse to capture local site effects in the expected ground motions. However, the performance of site-response analyses that account for the local geotechnical soil properties of site-specific soil profiles, as for instance reported by Aguilar et al., (2019), is a computationally demanding task that is out of the scope of this study, but when integrated it could benefit the overall quality of seismic risk calculations for the study area. Complementary, we strongly advise the physical to generate exhaustive sets of cross-correlated-ground motion fields (at the required spectral periods by the buildings classes) to address their aleatory uncertainty. The selection of this model, among the available ones, carries epistemic uncertainties.

It is worth noting that the variability of the loss exceedance curves obtained for the cumulative damage (due to tsunamis) was derived from the damaged exposure models subjected to each realisation of cross-correlated ground motion fields (i.e., orange curves in Figure 12). Therefore, investigating the impact of other tsunami vulnerability and hazard data products (Behrens et al., 2021), which was beyond the scope of this paper, are nonetheless worth exploring. When such parametrisation in the tsunami data products becomes available for Lima, future studies could provide dimensionality of the contribution of the tsunami hazard upon the outlined method for scenario multi-risk estimates.

For the commonly exposed residential building stock of Lima exposed to both perils, we have observed that assuming initial undamaged states in the selected tsunami empirical fragility functions leads to large underestimations for lower magnitudes (M_w) and large overestimations for larger M_w events in comparison to when state-dependent models were used. Hence, the initial "undamaged state" assumption used to assess the tsunami vulnerability in former studies (e.g., Adriano et al., 2014; Gómez Zapata et al., 2021e) may not be completely accurate to represent the losses expected after this type of cascading sequence. This is because such an assumption misses the calculation of earthquake-related damage which is an

https://doi.org/10.5194/nhess-2022-183
Preprint. Discussion started: 6 July 2022

important input needed to assess cumulative damage and losses through state-dependent analytical fragility models. On the other hand, adopting the larger value between independent earthquake and tsunami risk computations proposed by Goda and De Risi, (2018) may lead to better correspondence with our model (mostly for the lower M_w events) than the sole use of the selected non-state dependent analytical fragility functions.

6 Conclusions

We have proposed a modular method that allows us to consistently re-use existing single hazard fragility models that are being developed by experts in various research fields and integrate each other for multi-hazard risk assessment for extended building portfolios. This integration aims for the probabilistic harmonisation of diverse hazard-dependent building classes and damage states which are included in their associated fragility functions. Through this integration, we aim to provide an alternative approach to conventional ones (e.g., HAZUS-MH (FEMA, 2003, 2017)) that consider a single building class with sets of fragility functions for a variety of hazards. In this sense, the method we have developed can be particularly useful to assess the cumulative damage in hazard sequences of different natures and forces that might induce various failure mechanisms upon the exposed buildings. Thereby, the presented integrative method contributes to reducing the existing gaps due to the typical lack of collective calibration and validation of multi-hazard risk methods. This is due, for instance, when triggered events act on damaged assets right after the first hazard or even simultaneously experiencing compound hazards with no time for damage reconnaissance or disaggregation of the damage features induced by the individual hazards.

We have proposed a modular method composed of the following components:

1. The selection of existing hazard-dependent vulnerability schemes to model the building portfolio under each hazard-dependent vulnerability scheme of interest. They contain sets of building classes and associated fragility functions. To model the physical vulnerability of the building portfolio towards the triggering event (in this case, earthquake), no preference on whether empirical or analytical fragility functions should be used.
2. On the other hand, to model the physical vulnerability of the building stock towards the triggered event, sets of state-dependent fragility functions must be derived for each building type within the selected scheme. For this purpose, it is important to use models that do not involve the damaging effects of the triggered event as the starting point. (i.e., avoiding empirical models and using analytical ones). This proposal overcomes the assumption of initial undamaged states for the structures exposed to the triggered event and allows to account for the differential cumulative damage between hazards.
3. The characterisation of building classes through their disaggregation into building taxonomic attributes. This description allows the harmonisation between the building classes belonging to different hazard-dependent vulnerability schemes through the probabilistic inter-scheme compatibility matrix proposed in Gómez Zapata et al., (2022b).

https://doi.org/10.5194/nhess-2022-183
Preprint. Discussion started: 6 July 2022


Natural Hazards and Earth System Sciences Discussions

4. The exposure models are spatially aggregated into optimal geographic entities (i.e. CVT-based models) that account for the spatial variability of low-correlated hazard IM in their derivation (Gómez Zapata et al., 2021e). This selection was taken due to performance purposes only, but a more refined block-based model could also have been used.
5. A generalized description of the damage states based on a set of observable damage types on individual building components. This is done through a scoring system based on an underlying common scale (employing, for example, the AeDES form) that ultimately allows us to get the damage-state inter-scheme conversion. We use the total probability theorem, a Bayesian formulation, and machine learning techniques.
6. The vulnerability assessment for sequences of cascading hazards scenarios through the proposal of consistent economical consequence models across hazard-dependent vulnerability schemes. They must define replacement cost ratios per damage state and per fragility function associated with each vulnerability scheme.

The joint combination of these components creates a method to update the damage states throughout the multi-hazard sequence while allowing us to exploit existing hazard-specific risk-oriented taxonomies (i.e., building classifications with corresponding fragility functions and defined damage states) available in the literature for a wide range of natural hazards. This is a modular method in which each one of their individual components can be separately customized when seeking future improvements.

When applying this method on the residential building stock of Lima (Peru), we have observed, on the one hand, that considering the risk metrics from tsunami vulnerability only from the selected set of empirical fragility functions (derived from near-field tsunamis) as representative of the shaking and tsunami sequences leads to underestimations for the lower magnitudes. On the other hand, we have observed overestimations for the larger magnitude scenarios in comparison with the state-dependent method that accounts for the accumulated damage due to the former earthquake solicitations. We have observed that the use of the proposed method to assess the cumulative damage is more relevant for the lower magnitude scenarios than we have considered (M_w 8.5 and 8.6). This might be due to the greater damage extension on the exposed buildings that is expected from the seismic demands in comparison with those imposed by their corresponding tsunamis, and thus, there is greater chance to obtain cumulative damage. On the contrary, for larger magnitudes, the use of state-dependent fragilities and analytical functions assuming no pre-existing damage are converging, and thus, the importance of assessing state-dependency is reduced.

Considering the limitations and simplifications assumed in this study, we are not claiming that the resulting economic losses we have calculated for the residential building stock of Lima from multi-hazard scenario-based risk computations are totally exhaustive. Thus, caution should be taken with the interpretation and extrapolation of these conclusions to other study areas and combinations of models. Nevertheless, awareness of these uncertainties for the reliable quantification of risk towards these cascading hazards is increasingly important to enhance mitigation strategies for disaster risk reduction (Imamura et al., 2019). Furthermore, it is worth recalling that the method herein proposed has been exclusively designed for spatially extended residential building buildings as a proof of concept for integrating existing fragility models. We do not provide an\ complete

https://doi.org/10.5194/nhess-2022-183
Preprint. Discussion started: 6 July 2022

validation of multi-vulnerabilities approaches, but rather we offer a holistic and novel harmonising method to track such dynamics in a consistent manner. Hence, our method is not meant to replace more detailed analytical analyses required to determine the structural response of individual buildings subjected to seismic and tsunami loading (e.g., Petrone et al., 2017; Rossetto et al., 2019).

650

Code and data availability. The data used in the elaboration of this study are available in open repositories. The scenario-based ground motions and tsunami inundation maps are available in Gómez Zapata et al., (2021c); Harig and Rakowsky, (2021), respectively. The first set was calculated making use of the Shakyground script (Weatherill et al., 2021) which relies on the OpenQuake Engine (Pagani et al., 2014), whilst the second set was calculated using the TsunAWI software. The exposure and fragility models for both hazard-vulnerability
655 schemes (earthquake and tsunami) are available in Gómez Zapata et al., (2021a, b) and were adapted to fulfil the data formats required by the scripts provided by Assetmaster and Modelprop (Pittore et al., 2021). They were used as inputs for the scenario-based seismic risk assessment (Sect. 3.6) using the DEUS software (Brinckmann et al., 2021). The scenario-based risk estimates for earthquakes and tsunami using analytical and empirical fragility functions respectively are provided in Gómez Zapata et al., (2021d). State-dependent analytical tsunami fragility functions used in this study are available in Gómez Zapata et al., (2022a). The set of inter-scheme damage compatibility
660 matrices used in this study are provided in Gómez Zapata et al., (2022c).

Competing interests. The authors declare that they have no conflict of interest. The funders had no role in the design of the study; in the collection, analysis, or interpretation of the data; in the writing of the manuscript; or in the decision to publish the results.

Funding. This research was funded by the RIESGOS and RIESGOS 2.0 projects, funded by the German Federal Ministry of Education and Research (BMBF), with Grant No. 03G0876A-J and 03G0905A-H, respectively. These projects are part of the funding programme CLIENT
665 II – International Partnerships for Sustainable Innovations'.

Acknowledgments. The authors want to express their gratitude to Andrey Babeyko, Michael Haas, Michael Langbein, Giuseppe Nicodemo, Cecilia Nievas, Juan Páez-Ramírez, Juan Palomino, Matthias Rüster, and Sandra Santa-Cruz for their support during the elaboration of this study. Thanks to Sven Harig and Natalja Rakowsky for having provided us with the tsunami inundation models for Lima. We also thank Henning Lilienkamp and Graeme Weatherill for their support with the simulation of spatially correlated ground motion fields and machine
670 learning techniques. We thank Kevin Fleming for the careful proofreading.

References

Adriano, B., Mas, E., Koshimura, S., Estrada, M., and Jimenez, C.: Scenarios of Earthquake and Tsunami Damage Probability in Callao Region, Peru Using Tsunami Fragility Functions, J. Disaster Res., 9, 968–975, https://doi.org/10.20965/jdr.2014.p0968, 2014.

Aguilar, Z., Lazares, F., Alarcon, S., Quispe, S., Uriarte, R., and Calderon, D.: Actualización de la Microzonificación Sísmica de la ciudad
675 de Lima, International Symposium for CISMID 25th Anniversary 17–18 August, 2012, Lima, Peru, 2013.

Aguilar, Z., Tarazona, J., Vergaray, L., Barrantes, J., Uriarte, R., and Calderon, D.: Site response analysis and its comparison with the peruvian seismic design spectrum, TECNIA, 29, n.º 2, ago. 2019, https://doi.org/10.21754/tecnia.v29i2.700, 2019.

https://doi.org/10.5194/nhess-2022-183
Preprint. Discussion started: 6 July 2022

Allen, T. I. and Wald, D. J.: Topographic Slope as a Proxy for Seismic Site-Conditions (VS30) and Amplification Around the Globe, https://doi.org/10.3133/ofr20071357, 2007.

Antoncecchi, I., Ciccone, F., Dialuce, G., Grandi, S., Terlizzeze, F., Di Bucci, D., Dolce, M., Argnani, A., Mercorella, A., Pellegrini, C., Rovere, M., Armigliato, A., Pagnoni, G., Paparo, M. A., Tinti, S., Zaniboni, F., Basili, R., Cavallaro, D., Coltelli, M., Firetto Carlino, M., Lipparini, L., Lorito, S., Maesano, F. E., Romano, F., Scarfi, L., Tiberti, M. M., Volpe, M., Fedorik, J., Toscani, G., Borzi, B., Faravelli, M., Bozzoni, F., Pascale, V., Quaroni, D., Germagnoli, F., Belliazzi, S., Del Zoppo, M., Di Ludovico, M., Lignola, G. P., and Prota, A.: Progetto SPOT - Sismicità Potenzialmente Innescabile Offshore e Tsunami: Report integrato di fine progetto, 1. Ministero dello Sviluppo Economico, https://doi.org/10.5281/zenodo.3732887, 2020.

Arrighi, C., Tanganelli, M., Cristofaro, M. T., Cardinali, V., Marra, A., Castelli, F., and De Stefano, M.: Multi-risk assessment in a historical city, Nat. Hazards, https://doi.org/10.1007/s11069-021-05125-6, 2022.

Attary, N., van de Lindt, J. W., Unnikrishnan, V. U., Barbosa, A. R., and Cox, D. T.: Methodology for Development of Physics-Based Tsunami Fragilities, J. Struct. Eng., 143, 04016223, https://doi.org/10.1061/(ASCE)ST.1943-541X.0001715, 2017.

Attary, N., Van De Lindt, J. W., Barbosa, A. R., Cox, D. T., and Unnikrishnan, V. U.: Performance-Based Tsunami Engineering for Risk Assessment of Structures Subjected to Multi-Hazards: Tsunami following Earthquake, J. Earthq. Eng., 1–20, https://doi.org/10.1080/13632469.2019.1616335, 2019.

Baggio, C., Bernardini, A., Colozza, R., Corazza, L., Della Orsini, M., Di Pascuale, G., Dolce, M., Goretti, A., Martinelli, A., Orsini, G., Papa, F., and Zuccaro, G.: Field Manual for post-earthquake damage and safety assessment and short term countermeasures (AeDES), EUR 22868 EN – Joint Research Centre – Institute for the Protection and Security of the Citizen., : Office for Official Publications of the European Communities, Luxembourg, 100 pp. – 21.00 x 29.70 cm pp., 2007.

Behrens, J., Løvholt, F., Jalayer, F., Lorito, S., Salgado-Gálvez, M. A., Sørensen, M., Abadie, S., Aguirre-Ayerbe, I., Aniel-Quiroga, I., Babeyko, A., Baiguera, M., Basili, R., Belliazzi, S., Grezio, A., Johnson, K., Murphy, S., Paris, R., Rafliana, I., De Risi, R., Rossetto, T., Selva, J., Taroni, M., Del Zoppo, M., Armigliato, A., Bureš, V., Cech, P., Cecioni, C., Christodoulides, P., Davies, G., Dias, F., Bayraktar, H. B., González, M., Gritsevich, M., Guillas, S., Harbitz, C. B., Kânoğlu, U., Macías, J., Papadopoulos, G. A., Polet, J., Romano, F., Salamon, A., Scala, A., Stepinac, M., Tappin, D. R., Thio, H. K., Tonini, R., Triantafyllou, I., Ulrich, T., Varini, E., Volpe, M., and Vyhmeister, E.: Probabilistic Tsunami Hazard and Risk Analysis: A Review of Research Gaps, Front. Earth Sci., 9, https://doi.org/10.3389/feart.2021.628772, 2021.

Belliazzi, S., Lignola, G. P., Di Ludovico, M., and Prota, A.: Preliminary tsunami analytical fragility functions proposal for Italian coastal residential masonry buildings, Structures, 31, 68–79, https://doi.org/10.1016/j.istruc.2021.01.059, 2021.

Bernal, G. A., Salgado-Gálvez, M. A., Zuloaga, D., Tristancho, J., González, D., and Cardona, O.-D.: Integration of Probabilistic and Multi-Hazard Risk Assessment Within Urban Development Planning and Emergency Preparedness and Response: Application to Manizales, Colombia, Int. J. Disaster Risk Sci., 8, 270–283, https://doi.org/10.1007/s13753-017-0135-8, 2017.

Bonacho, J. and Oliveira, C. S.: Multi-hazard analysis of earthquake shaking and tsunami impact, Int. J. Disaster Risk Reduct., 31, 275–280, https://doi.org/10.1016/j.ijdrr.2018.05.023, 2018.

Brinckmann, N., Gomez-Zapata, J. C., Pittore, M., and Rüster, M.: DEUS: Damage-Exposure-Update-Service. V. 1.0., GFZ Data Serv., https://doi.org/10.5880/riesgos.2021.011, 2021.

Brzev, S., Scawthor, C., Charleson, AW., Allen, L., Greene, M., Jaiswal, K., and Silva, V.: GEM building taxonomy version 2.0, GEM Foundation, Pavia, 2013.

Buitinck, L., Louppe, G., Blondel, M., Pedregosa, F., Mueller, A., Grisel, O., Niculae, V., Prettenhofer, P., Gramfort, A., Grobler, J., Layton, R., VanderPlas, J., Joly, A., Holt, B., and Varoquaux, G.: API design for machine learning software: experiences from the scikit-learn project, in: ECML PKDD Workshop: Languages for Data Mining and Machine Learning, 108–122, 2013.

https://doi.org/10.5194/nhess-2022-183
Preprint. Discussion started: 6 July 2022

Ceferino, L., Kiremidjian, A., and Deierlein, G.: Regional Multiseverity Casualty Estimation Due to Building Damage following a Mw 8.8 Earthquake Scenario in Lima, Peru, Earthq. Spectra, 34, 1739–1761, https://doi.org/10.1193/080617EQS154M, 2018.

Charvet, I., Macabuag, J., and Rossetto, T.: Estimating Tsunami-Induced Building Damage through Fragility Functions: Critical Review and Research Needs, Front. Built Environ., 3, 36, https://doi.org/10.3389/fbuil.2017.00036, 2017.

Cremen, G., Galasso, C., and McCloskey, J.: Modelling and quantifying tomorrow's risks from natural hazards, Sci. Total Environ., 817, 152552, https://doi.org/10.1016/j.scitotenv.2021.152552, 2022.

Dabbeek, J. and Silva, V.: Modeling the residential building stock in the Middle East for multi-hazard risk assessment, Nat. Hazards, 100, 781–810, https://doi.org/10.1007/s11069-019-03842-7, 2020.

Dabbeek, J., Silva, V., Galasso, C., and Smith, A.: Probabilistic earthquake and flood loss assessment in the Middle East, Int. J. Disaster Risk Reduct., 49, 101662, https://doi.org/10.1016/j.ijdrr.2020.101662, 2020.

Daniell, J. E., Schaefer, A. M., and Wenzel, F.: Losses Associated with Secondary Effects in Earthquakes, Front. Built Environ., 3, 30, https://doi.org/10.3389/fbuil.2017.00030, 2017.

De Angeli, S., Malamud, B. D., Rossi, L., Taylor, F. E., Trasforini, E., and Rudari, R.: A multi-hazard framework for spatial-temporal impact analysis, Int. J. Disaster Risk Reduct., 102829, https://doi.org/10.1016/j.ijdrr.2022.102829, 2022.

Del Zoppo, M., Wijesundara, K., Rossetto, T., Dias, P., Baiguera, M., Ludovico, M. D., Thamboo, J., and Prota, A.: Influence of exterior infill walls on the performance of RC frames under tsunami loads: Case study of school buildings in Sri Lanka, Eng. Struct., 234, 111920, https://doi.org/10.1016/j.engstruct.2021.111920, 2021.

Dorbath, L., Cisternas, A., and Dorbath, C.: Assessment of the size of large and great historical earthquakes in Peru, Bull. Seismol. Soc. Am., 80, 551–576, 1990.

FEMA: Multi-hazard loss estimation methodology, Federal Emergency Management Agency, Washington, 2003.

FEMA: HAZUS Tsunami Model Technical Guidance, Federal Emergency Management Agency, Washington, D.C., 2017.

Figueiredo, R., Romão, X., and Paupério, E.: Component-based flood vulnerability modelling for cultural heritage buildings, Int. J. Disaster Risk Reduct., 61, 102323, https://doi.org/10.1016/j.ijdrr.2021.102323, 2021.

Frucht, E., Salamon, A., Rozelle, J., Levi, T., Calvo, R., Avirav, V., Burns, J. N., Zuzak, C., Gal, E., Trapper, P., Galanti, B., and Bausch, D.: Tsunami loss assessment based on Hazus approach – The Bat Galim, Israel, case study, Eng. Geol., 289, 106175, https://doi.org/10.1016/j.enggeo.2021.106175, 2021.

Gallina, V., Torresan, S., Critto, A., Sperotto, A., Glade, T., and Marcomini, A.: A review of multi-risk methodologies for natural hazards: Consequences and challenges for a climate change impact assessment, J. Environ. Manage., 168, 123–132, https://doi.org/10.1016/j.jenvman.2015.11.011, 2016.

Gehl, P. and D'Ayala, D.: System loss assessment of bridge networks accounting for multi-hazard interactions, Struct. Infrastruct. Eng., 14, 1355–1371, https://doi.org/10.1080/15732479.2018.1434671, 2018.

Gehl, P., Quinet, C., Le Cozannet, G., Kouokam, E., and Thierry, P.: Potential and limitations of risk scenario tools in volcanic areas through an example at Mount Cameroon, Nat. Hazards Earth Syst. Sci., 13, 2409–2424, https://doi.org/10.5194/nhess-13-2409-2013, 2013.

GEM: Report on the SARA Exposure and Vulnerability Workshop in Medellin, Colombia, 2014.

Gill, J. C. and Malamud, B. D.: Reviewing and visualizing the interactions of natural hazards, Rev. Geophys., 52, 680–722, https://doi.org/10.1002/2013RG000445, 2014.

https://doi.org/10.5194/nhess-2022-183
Preprint. Discussion started: 6 July 2022

Gill, J. C. and Malamud, B. D.: Hazard interactions and interaction networks (cascades) within multi-hazard methodologies, Earth Syst. Dyn., 7, 659–679, https://doi.org/10.5194/esd-7-659-2016, 2016.

Goda, K. and De Risi, R.: Multi-hazard loss estimation for shaking and tsunami using stochastic rupture sources, Int. J. Disaster Risk Reduct., 28, 539–554, https://doi.org/10.1016/j.ijdrr.2018.01.002, 2018.

Goda, K., Mori, N., Yasuda, T., Prasetyo, A., Muhammad, A., and Tsujio, D.: Cascading Geological Hazards and Risks of the 2018 Sulawesi Indonesia Earthquake and Sensitivity Analysis of Tsunami Inundation Simulations, Front. Earth Sci., 7, 261, https://doi.org/10.3389/feart.2019.00261, 2019.

Gómez Zapata, J. C., Pittore, M., Brinckmann, N., and Shinde, S.: Dynamic physical vulnerability: a Multi-risk Scenario approach from building- single- hazard fragility- models, in: EGU General Assembly Conference Abstracts, Online, 18379, 2020.

Gómez Zapata, J. C., Zafrir, R., Harig, S., and Pittore, M.: Customised focus maps and resultant CVT-based aggregation entities for Lima and Callao (Peru). V. 1.0., GFZ Data Serv., https://doi.org/10.5880/riesgos.2021.006, 2021a.

Gómez Zapata, J. C., Zafrir, R., Brinckmann, N., and Pittore, M.: Residential building exposure and physical vulnerability models for ground-shaking and tsunami risk in Lima and Callao (Peru). V. 1.0., GFZ Data Serv., https://doi.org/10.5880/riesgos.2021.007, 2021b.

Gómez Zapata, J. C., Brinckmann, N., Pittore, M., and Cotton, F.: Seismic ground motion fields for six deterministic earthquake scenarios (Mw 8.5-9.0) for Lima (Peru), GFZ Data Serv., https://doi.org/10.5880/riesgos.2021.008, 2021c.

Gómez Zapata, J. C., Brinckmann, N., Pittore, M., and Cotton, F.: Spatial representation of direct loss estimates on the residential building stock of Lima (Peru) from decoupled earthquake and tsunami scenarios on variable resolutions exposure models., GFZ Data Serv., https://doi.org/10.5880/riesgos.2021.009, 2021d.

Gómez Zapata, J. C., Brinckmann, N., Harig, S., Zafrir, R., Pittore, M., Cotton, F., and Babeyko, A.: Variable-resolution building exposure modelling for earthquake and tsunami scenario-based risk assessment. An application case in Lima, Peru, Nat. Hazards Earth Syst. Sci., 21, 3599–3628, https://doi.org/10.5194/nhess-21-3599-2021, 2021e.

Gómez Zapata, J. C., Medina, S., and Lizarazo-Marriaga, J.: Creation of simplified state-dependent fragility functions through ad-hoc scaling factors to account for previous damage in a multi-hazard risk context. An application to flow-depth-based analytical tsunami fragility functions for the Pacific coast of South America, GFZ Data Serv., 2022a. Review link: https://dataservices.gfz-potsdam.de/panmetaworks/review/b1e611344f04b57fa73d31e48f5b482cda74afa8254c5685ad0fe4f97d3f8c6c/

Gómez Zapata, J. C., Pittore, M., Cotton, F., Lilienkamp, H., Simantini, S., Aguirre, P., and Hernan, S. M.: Epistemic uncertainty of probabilistic building exposure compositions in scenario-based earthquake loss models, Bull. Earthq. Eng., https://doi.org/10.1007/s10518-021-01312-9, 2022b.

Gómez Zapata, J. C., Pittore, M., and Juan: Probabilistic inter-scheme compatibility matrices for multi-hazard exposure modeling. An application using existing vulnerability models for earthquakes and tsunami from synthetic datasets constructed using the AeDEs form through expert-based heuristics, GFZ Data Serv., https://doi.org/10.5880/riesgos.2022.003, 2022c. Review link https://dataservices.gfz-potsdam.de/panmetaworks/review/6355f1be60969620c71b09b4ff4595d9f3d2247b30260a49cce816c9f5f41e0d/

Grünthal, G.: European Macroseismic Scale 1998, Centre Européen de Géodynamique et de Séismologie., Luxembourg, 1998.

Harig, S. and Rakowsky, N.: Tsunami flow depth in Lima/Callao (Peru) caused by six hypothetical simplified tsunami scenarios offshore Lima, GFZ Data Serv., https://doi.org/10.5880/riesgos.2021.010, 2021.

Harig, S., Immerz, A., Weniza, Griffin, J., Weber, B., Babeyko, A., Rakowsky, N., Hartanto, D., Nurokhim, A., Handayani, T., and Weber, R.: The Tsunami Scenario Database of the Indonesia Tsunami Early Warning System (InaTEWS): Evolution of the Coverage and the Involved Modeling Approaches, Pure Appl. Geophys., 177, 1379–1401, https://doi.org/10.1007/s00024-019-02305-1, 2020.

https://doi.org/10.5194/nhess-2022-183
Preprint. Discussion started: 6 July 2022

Hill, M. and Rossetto, T.: Comparison of building damage scales and damage descriptions for use in earthquake loss modelling in Europe, Bull. Earthq. Eng., 6, 335–365, https://doi.org/10.1007/s10518-007-9057-y, 2008.

Imamura, F., Boret, S. P., Suppasri, A., and Muhari, A.: Recent occurrences of serious tsunami damage and the future challenges of tsunami disaster risk reduction, Prog. Disaster Sci., 1, 100009, https://doi.org/10.1016/j.pdisas.2019.100009, 2019.

INEI: Censos Nacionales 2017, Instituto Nacional de Estadistica e Informatica (INEI; Institute of Statistic and Informatics), Lima, Peru, 2017.

Jimenez, C., Moggiano, N., Mas, E., Adriano, B., Koshimura, S., Fujii, Y., and Yanagisawa, and H.: Seismic Source of 1746 Callao Earthquake from Tsunami Numerical Modeling, J. Disaster Res., 8, 266–273, https://doi.org/10.20965/jdr.2013.p0266, 2013.

Julià, P. B. and Ferreira, T. M.: From single- to multi-hazard vulnerability and risk in Historic Urban Areas: a literature review, Nat. Hazards, 108, 93–128, https://doi.org/10.1007/s11069-021-04734-5, 2021.

Kappes, M. S., Keiler, M., von Elverfeldt, K., and Glade, T.: Challenges of analyzing multi-hazard risk: a review, Nat. Hazards, 64, 1925–1958, https://doi.org/10.1007/s11069-012-0294-2, 2012.

Karapetrou, S., Manakou, M., Bindi, D., Petrovic, B., and Pitilakis, K.: "Time-building specific" seismic vulnerability assessment of a hospital RC building using field monitoring data, Eng. Struct., 112, 114–132, https://doi.org/10.1016/j.engstruct.2016.01.009, 2016.

Komendantova, N., Mrzyglocki, R., Mignan, A., Khazai, B., Wenzel, F., Patt, A., and Fleming, K.: Multi-hazard and multi-risk decision-support tools as a part of participatory risk governance: Feedback from civil protection stakeholders, Int. J. Disaster Risk Reduct., 8, 50–67, https://doi.org/10.1016/j.ijdrr.2013.12.006, 2014.

Kulikov, E. A., Rabinovich, A. B., and Thomson, R. E.: Estimation of Tsunami Risk for the Coasts of Peru and Northern Chile, Nat. Hazards, 35, 185–209, https://doi.org/10.1007/s11069-004-4809-3, 2005.

Lagomarsino, S. and Giovinazzi, S.: Macroseismic and mechanical models for the vulnerability and damage assessment of current buildings, Bull. Earthq. Eng., 4, 415–443, https://doi.org/10.1007/s10518-006-9024-z, 2006.

Lagomarsino, S., Cattari, S., and Ottonelli, D.: The heuristic vulnerability model: fragility curves for masonry buildings, Bull. Earthq. Eng., 19, 3129–3163, https://doi.org/10.1007/s10518-021-01063-7, 2021.

Lahcene, E., Ioannou, I., Suppasri, A., Pakoksung, K., Paulik, R., Syamsidik, S., Bouchette, F., and Imamura, F.: Characteristics of building fragility curves for seismic and non-seismic tsunamis: case studies of the 2018 Sunda Strait, 2018 Sulawesi-Palu and 2004 Indian Ocean tsunamis, Nat. Hazards Earth Syst. Sci., 2020, 1–36, https://doi.org/10.5194/nhess-21-2313-2021, 2021.

Liu, B., Siu, Y. L., and Mitchell, G.: Hazard interaction analysis for multi-hazard risk assessment: a systematic classification based on hazard-forming environment, Nat. Hazards Earth Syst. Sci., 16, 629–642, https://doi.org/10.5194/nhess-16-629-2016, 2016.

Løvholt, F., Glimsdal, S., Harbitz, C. B., Horspool, N., Smebye, H., Bono, A. de, and Nadim, F.: Global tsunami hazard and exposure due to large co-seismic slip, Int. J. Disaster Risk Reduct., 10, 406–418, https://doi.org/10.1016/j.ijdrr.2014.04.003, 2014.

Maiwald, H. and Schwarz, J.: Unified damage description and risk assessment of buildings under extreme natural hazards, Mauerwerk, 23, 95–111, https://doi.org/10.1002/dama.201910014, 2019.

Mangalathu, S., Sun, H., Nweke, C. C., Yi, Z., and Burton, H. V.: Classifying earthquake damage to buildings using machine learning, Earthq. Spectra, 36, 183–208, https://doi.org/10.1177/8755293019878137, 2020.

Markhvida, M., Ceferino, L., and Baker, J. W.: Modeling spatially correlated spectral accelerations at multiple periods using principal component analysis and geostatistics, Earthq. Eng. Struct. Dyn., 47, 1107–1123, https://doi.org/10.1002/eqe.3007, 2018.

https://doi.org/10.5194/nhess-2022-183
Preprint. Discussion started: 6 July 2022

Marzocchi, W., Garcia-Aristizabal, A., Gasparini, P., Mastellone, M. L., and Di Ruocco, A.: Basic principles of multi-risk assessment: a case study in Italy, Nat. Hazards, 62, 551–573, https://doi.org/10.1007/s11069-012-0092-x, 2012.

Mas, E., Paulik, R., Pakoksung, K., Adriano, B., Moya, L., Suppasri, A., Muhari, A., Khomarudin, R., Yokoya, N., Matsuoka, M., and Koshimura, S.: Characteristics of Tsunami Fragility Functions Developed Using Different Sources of Damage Data from the 2018 Sulawesi Earthquake and Tsunami, Pure Appl. Geophys., 177, 2437–2455, https://doi.org/10.1007/s00024-020-02501-4, 2020.

Medina, S.: Zonificación de la vulnerabilidad física para edificaciones típicas en San Andrés de Tumaco, Costa Pacífica Colombiana, Master thesis in Civil Engineering, Universidad Nacional de Colombia Facultad de Ingeniería, Departamento Ingeniería Civil y Ambiental, Bogotá, Colombia, 245 pp., 2019.

Medina, S., Lizarazo-Marriaga, J., Estrada, M., Koshimura, S., Mas, E., and Adriano, B.: Tsunami analytical fragility curves for the Colombian Pacific coast: A reinforced concrete building example, Eng. Struct., 196, 109309, https://doi.org/10.1016/j.engstruct.2019.109309, 2019.

Merz, B., Kuhlicke, C., Kunz, M., Pittore, M., Babeyko, A., Bresch, D. N., Domeisen, D. I. V., Feser, F., Koszalka, I., Kreibich, H., Pantillon, F., Parolai, S., Pinto, J. G., Punge, H. J., Rivalta, E., Schröter, K., Strehlow, K., Weisse, R., and Wurpts, A.: Impact Forecasting to Support Emergency Management of Natural Hazards, Rev. Geophys., 58, e2020RG000704, https://doi.org/10.1029/2020RG000704, 2020.

Mignan, A., Wiemer, S., and Giardini, D.: The quantification of low-probability–high-consequences events: part I. A generic multi-risk approach, Nat. Hazards, 73, 1999–2022, https://doi.org/10.1007/s11069-014-1178-4, 2014.

Montalva, G. A., Bastías, N., and Rodriguez-Marek, A.: Ground-Motion Prediction Equation for the Chilean Subduction Zone, Bull. Seismol. Soc. Am., 107, 901–911, https://doi.org/10.1785/0120160221, 2017.

Negulescu, C., Benaïchouche, A., Lemoine, A., Le Roy, S., and Pedreros, R.: Adjustability of exposed elements by updating their capacity for resistance after a damaging event: application to an earthquake–tsunami cascade scenario, Nat. Hazards, 104, 753–793, https://doi.org/10.1007/s11069-020-04189-0, 2020.

Ordaz, M., Salgado-Gálvez Mario Andrés, Huerta Benjamín, Rodríguez Juan Carlos, and Avelar Carlos: Considering the impacts of simultaneous perils: The challenges of integrating earthquake and tsunamigenic risk, Disaster Prev. Manag. Int. J., 28, 823–837, https://doi.org/10.1108/DPM-09-2019-0295, 2019.

Pagani, M., Monelli, D., Weatherill, G., Danciu, L., Crowley, H., Silva, V., Henshaw, P., Butler, L., Nastasi, M., Panzeri, L., Simionato, M., and Vigano, D.: OpenQuake Engine: An Open Hazard (and Risk) Software for the Global Earthquake Model, Seismol. Res. Lett., 85, 692–702, https://doi.org/10.1785/0220130087, 2014.

Papadopoulos, A. N. and Bazzurro, P.: Exploring probabilistic seismic risk assessment accounting for seismicity clustering and damage accumulation: Part II. Risk analysis, Earthq. Spectra, 37, 386–408, https://doi.org/10.1177/8755293020938816, 2021.

Park, H., Cox, D. T., and Barbosa, A. R.: Comparison of inundation depth and momentum flux based fragilities for probabilistic tsunami damage assessment and uncertainty analysis, Coast. Eng., 122, 10–26, https://doi.org/10.1016/j.coastaleng.2017.01.008, 2017.

Park, H., Alam, M. S., Cox, D. T., Barbosa, A. R., and Lindt, J. W. van de: Probabilistic seismic and tsunami damage analysis (PSTDA) of the Cascadia Subduction Zone applied to Seaside, Oregon, Int. J. Disaster Risk Reduct., 35, 101076, https://doi.org/10.1016/j.ijdrr.2019.101076, 2019.

Pescaroli, G. and Alexander, D.: Understanding Compound, Interconnected, Interacting, and Cascading Risks: A Holistic Framework, Risk Anal., 38, 2245–2257, https://doi.org/10.1111/risa.13128, 2018.

Petersen, M. D., Harmsen, S. C., Jaiswal, K. S., Rukstales, K. S., Luco, N., Haller, K. M., Mueller, C. S., and Shumway, A. M.: Seismic Hazard, Risk, and Design for South America, Bull. Seismol. Soc. Am., 108, 781–800, https://doi.org/10.1785/0120170002, 2018.

https://doi.org/10.5194/nhess-2022-183
Preprint. Discussion started: 6 July 2022

Petrone, C., Rossetto, T., and Goda, K.: Fragility assessment of a RC structure under tsunami actions via nonlinear static and dynamic analyses, Eng. Struct., 136, 36–53, https://doi.org/10.1016/j.engstruct.2017.01.013, 2017.

Petrone, C., Rossetto, T., Baiguera, M., la Barra Bustamante, C. D., and Ioannou, I.: Fragility functions for a reinforced concrete structure subjected to earthquake and tsunami in sequence, Eng. Struct., 205, 110120, https://doi.org/10.1016/j.engstruct.2019.110120, 2020.

Pittore, M., Haas, M., and Megalooikonomou, K. G.: Risk-Oriented, Bottom-Up Modeling of Building Portfolios With Faceted Taxonomies, Front. Built Environ., 4, 41, https://doi.org/10.3389/fbuil.2018.00041, 2018.

Pittore, M., Haas, M., and Silva, V.: Variable resolution probabilistic modeling of residential exposure and vulnerability for risk applications, Earthq. Spectra, 36, 321–344, https://doi.org/10.1177/8755293020951582, 2020.

Pittore, M., Gomez-Zapata, J. C., Brinckmann, N., and Rüster, M.: Assetmaster and Modelprop: web services to serve building exposure models and fragility functions for physical vulnerability to natural-hazards. V. 1.0, GFZ Data Serv., https://doi.org/10.5880/riesgos.2021.005, 2021.

Rossetto, T., Petrone, C., Eames, I., De La Barra, C., Foster, A., and Macabuag, J.: Advances in the Assessment of Buildings Subjected to Earthquakes and Tsunami, in: Recent Advances in Earthquake Engineering in Europe: 16th European Conference on Earthquake Engineering-Thessaloniki 2018, edited by: Pitilakis, K., Springer International Publishing, Cham, 545–562, https://doi.org/10.1007/978-3-319-75741-4_23, 2018.

Rossetto, T., De la Barra, C., Petrone, C., De la Llera, J. C., Vásquez, J., and Baiguera, M.: Comparative assessment of nonlinear static and dynamic methods for analysing building response under sequential earthquake and tsunami, Earthq. Eng. Struct. Dyn., 48, 867–887, https://doi.org/10.1002/eqe.3167, 2019.

de Ruiter, M. C., Couasnon, A., van den Homberg, M. J. C., Daniell, J. E., Gill, J. C., and Ward, P. J.: Why We Can No Longer Ignore Consecutive Disasters, Earths Future, 8, e2019EF001425, https://doi.org/10.1029/2019EF001425, 2020.

Schelske, O., Sundermann, L., and Hausmann, P.: Mind the risk - A global ranking of cities under threat from natural disasters, 2014.

Schwarz, J., Maiwald, H., Kaufmann, C., Langhammer, T., and Beinersdorf, S.: Conceptual basics and tools to assess the multi hazard vulnerability of existing buildings, Mauerwerk, 23, 246–264, https://doi.org/10.1002/dama.201910025, 2019.

Selva, J.: Long-term multi-risk assessment: statistical treatment of interaction among risks, Nat. Hazards, 67, 701–722, https://doi.org/10.1007/s11069-013-0599-9, 2013.

Silva, V., Yepes-Estrada, C., Dabbeek, J., Martins, L., and Brzev, S.: GED4ALL: Global exposure database for multi-hazard risk analysis. Multi-hazard exposure taxonomy, GEM Foundation, Pavia, 2018.

Silva, V., Brzev, S., Scawthorn, C., Yepes, C., Dabbeek, J., and Crowley, H.: A Building Classification System for Multi-hazard Risk Assessment, Int. J. Disaster Risk Sci., https://doi.org/10.1007/s13753-022-00400-x, 2022.

Suppasri, A., Mas, E., Charvet, I., Gunasekera, R., Imai, K., Fukutani, Y., Abe, Y., and Imamura, F.: Building damage characteristics based on surveyed data and fragility curves of the 2011 Great East Japan tsunami, Nat. Hazards, 66, 319–341, https://doi.org/10.1007/s11069-012-0487-8, 2013.

Suppasri, A., Charvet, I., Imai, K., and Imamura, F.: Fragility Curves Based on Data from the 2011 Tohoku-Oki Tsunami in Ishinomaki City, with Discussion of Parameters Influencing Building Damage, Earthq. Spectra, 31, 841–868, https://doi.org/10.1193/053013EQS138M, 2015.

Suppasri, A., Maly, E., Kitamura, M., Syamsidik, Pescaroli, G., Alexander, D., and Imamura, F.: Cascading disasters triggered by tsunami hazards: A perspective for critical infrastructure resilience and disaster risk reduction, Int. J. Disaster Risk Reduct., 66, 102597, https://doi.org/10.1016/j.ijdrr.2021.102597, 2021.

Tarque, N., Salsavilca, J., Yacila, J., and Camata, G.: Multi-criteria analysis of five reinforcement options for Peruvian confined masonry walls, Earthq. Struct., 17, 205–219, 2019.

Terzi, S., Torresan, S., Schneiderbauer, S., Critto, A., Zebisch, M., and Marcomini, A.: Multi-risk assessment in mountain regions: A review of modelling approaches for climate change adaptation, J. Environ. Manage., 232, 759–771, https://doi.org/10.1016/j.jenvman.2018.11.100, 2019.

Tilloy, A., Malamud, B. D., Winter, H., and Joly-Laugel, A.: A review of quantification methodologies for multi-hazard interrelationships, Earth-Sci. Rev., 196, 102881, https://doi.org/10.1016/j.earscirev.2019.102881, 2019.

Trevlopoulos, K., Guéguen, P., Helmstetter, A., and Cotton, F.: Earthquake risk in reinforced concrete buildings during aftershock sequences based on period elongation and operational earthquake forecasting, Struct. Saf., 84, 101922, https://doi.org/10.1016/j.strusafe.2020.101922, 2020.

Triantafyllou, I., Novikova, T., Charalampakis, M., Fokaefs, A., and Papadopoulos, G. A.: Quantitative Tsunami Risk Assessment in Terms of Building Replacement Cost Based on Tsunami Modelling and GIS Methods: The Case of Crete Isl., Hellenic Arc, Pure Appl. Geophys., 176, 3207–3225, https://doi.org/10.1007/s00024-018-1984-9, 2019.

Turchi, A., Traglia, F. D., Gentile, R., Fornaciai, A., Zetti, I., and Fanti, R.: Relative seismic and tsunami risk assessment for Stromboli Island (Italy), Int. J. Disaster Risk Reduct., 76, 103002, https://doi.org/10.1016/j.ijdrr.2022.103002, 2022.

Vamvatsikos, D., Panagopoulos, G., Kappos, A. J., Nigro, E., Rossetto, T., Lloyd, T. O., and Stathopoulos, T.: Structural Vulnerability Assessment under Natural Hazards: A review, in: Urban Habitat Constructions under Catastrophic Events, CRC Press. Editor: Mazzolani, F.M, 2010.

Villar-Vega, M., Silva, V., Crowley, H., Yepes, C., Tarque, N., Acevedo, A. B., Hube, M. A., Gustavo, C. D., and María, H. S.: Development of a Fragility Model for the Residential Building Stock in South America, Earthq. Spectra, 33, 581–604, https://doi.org/10.1193/010716EQS005M, 2017.

Ward, P. J., Blauhut, V., Bloemendaal, N., Daniell, J. E., de Ruiter, M. C., Duncan, M. J., Emberson, R., Jenkins, S. F., Kirschbaum, D., Kunz, M., Mohr, S., Muis, S., Riddell, G. A., Schäfer, A., Stanley, T., Veldkamp, T. I. E., and Winsemius, H. C.: Review article: Natural hazard risk assessments at the global scale, Nat. Hazards Earth Syst. Sci., 20, 1069–1096, https://doi.org/10.5194/nhess-20-1069-2020, 2020.

Ward, P. J., Daniell, J., Duncan, M., Dunne, A., Hananel, C., Hochrainer-Stigler, S., Tijssen, A., Torresan, S., Ciurean, R., Gill, J., Sillmann, J., Couasnon, A., Koks, E., Padrón-Fumero, N., Tatman, S., Tronstad Lund, M., Adesiyun, A., Aerts, J., Alabaster, A., Butler, B., Campillo Torres, C., Critto, A., Hernández Martin, R., Machado, M., Mysiak, J., Orth, R., Palomino, I., Petrescu, E.-C., Reichstein, M., Tiggeloven, T., van Loon, A., Vuong Pham, H., and de Ruiter, M.: Invited perspectives: A research agenda towards disaster risk management pathways in multi-(hazard-)risk assessment, Nat. Hazards Earth Syst. Sci. Discuss., 2022, 1487–1497, https://doi.org/10.5194/nhess-22-1487-2022, 2022.

Weatherill, G., Pittore, M., Haas, M., Brinckmann, N., Rüster, M., and Gomez-Zapata, J. C.: Shakyground: a web service to serve GMPE-based ground motion fields. V. 1.0., GFZ Data Serv., https://doi.org/10.5880/riesgos.2021.004, 2021.

Yepes-Estrada, C., Silva, V., Valcárcel, J., Acevedo, A. B., Tarque, N., Hube, M. A., Coronel, G., and María, H. S.: Modeling the Residential Building Inventory in South America for Seismic Risk Assessment, Earthq. Spectra, 33, 299–322, https://doi.org/10.1193/101915EQS155DP, 2017.

Zuccaro, G., Cacace, F., Spence, R. J. S., and Baxter, P. J.: Impact of explosive eruption scenarios at Vesuvius, J. Volcanol. Geotherm. Res., 178, 416–453, https://doi.org/10.1016/j.jvolgeores.2008.01.005, 2008.

Zuccaro, G., De Gregorio, D., and Leone, M. F.: Theoretical model for cascading effects analyses, Underst. Mitigating Cascading Crises Glob. Interconnected Syst., 30, 199–215, https://doi.org/10.1016/j.ijdrr.2018.04.019, 2018.